LA-UR- 97-83
CONF-970160--1

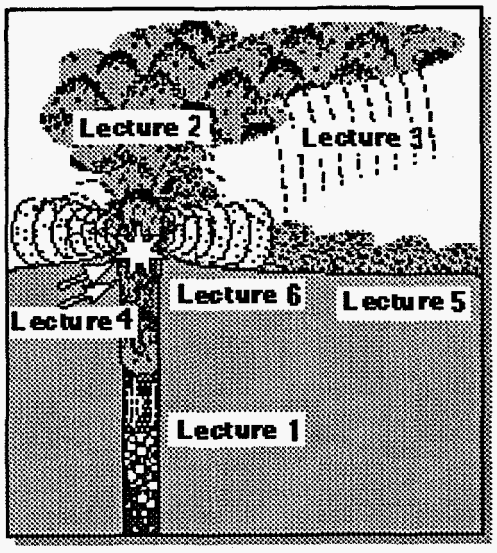

IAVCEI Commission on Explosive Volcanism
Short course on

THE PHYSICS OF EXPLOSIVE VOLCANISM

17-19 January, 1997
Puerto Vallarta, Mexico

Convened by Armin Freundt and Mauro Rosi

Lecture 2

Eruption column physics

by

Greg A. Valentine

Geoanalysis Group
Mail Stop F665
Los Alamos National Laboratory
Los Alamos, NM 87545
U.S.A.
phone: 505-665-0259
fax: 505-665-3687
email: gav@vega.Lanl.gov

DISCLAIMER

CONF-970160--1

Eruption Column Physics

Greg A. Valentine
Mail Stop F665, Geoanalysis Group
Los Alamos National Laboratory
Los Alamos, NM 87545 USA
email: gav@vega.lanl.gov

1. Introduction

Explosive volcanic eruptions consist of a clots and fragments of magma (molten or quenched to a solid state) and lithic material dispersed in a continuous gas phase. This mixture of gas, solids, and liquid is expelled vertically or subvertically from a vent as a jet with speeds up to a few hundred meters per second and a bulk density greater than that of the surrounding atmosphere. As a vertical or subvertical jet rises into the atmosphere its margins entrain air from the relatively cool atmosphere. This air is mixed into the the column, heated by the clasts in the eruptive mixture and expands, resulting in a net decrease in the mixture density. Simultaneously, the atmosphere exerts drag on the jet and gravity exerts a downward acceleration on it. The fate of the jet becomes subject to the competition between these processes. If sufficient air is entrained and heated the bulk density of the jet may decrease below that of the surrounding atmosphere. In this case the jet becomes buoyant and it continues rising as a plume, or a buoyant column, until it reaches a level of neutral buoyancy at which it spreads laterally in an "umbrella" cloud (Figure 1). However, if sufficient air is not entrained, the jet will continue to decelerate until at some altitude its velocity becomes zero. Since the bulk density at that altitude is still greater than the surrounding atmosphere, the mixture begins to fall back to the earth's surface. In this case the jet becomes a fountain, also called a collapsing column. Superimposed on all this are complicated multiphase effects such as condensation of water vapor and settling of large clasts, which feed back into the overall dynamics. All of these aspects of explosive eruptions, where flow is dominantly vertical whether it is up (jet and buoyant plume) or down (a collapsing column or fountain), are herein considered to define *eruption columns*.

Eruption columns come in a variety of shapes and sizes. On one end of the scale are basaltic fountains that may be as low as a few tens of meters. These may erupt from central vents, but more commonly erupt from long fissures to form linear fountains. Because the fountains are so low and the

erupting clasts are relatively large (cm to dm) there is very little heat loss from clasts and they tend to accumulate rapidly right around the vent. The still-molten clasts coalesce to form "clastogenic" lava flows that then move away from the vent. At somewhat higher gas contents and eruption velocities these fountains may grow to several hundred meters or higher. In general the higher the fountain, the more cooling of clasts during flight. For these higher fountains the clasts around the outer edge of the fountain may solidify in flight and therefore deposit as scoria (Figure 2). Relatively continuously-erupting fountains of this type and size are commonly referred to as *Hawaiian.* They are most common in basaltic eruptions, but also can occur in more silicic eruptions if magma viscosity is sufficiently low (for example, due to high alkali content).

Strombolian eruption columns are similar in size to Hawaiian ones, but tend to be more sporadic, characterized by short bursts of fountain activity separated by longer intervals of relative quiet. Clasts erupted in Strombolian columns are relatively coarse and have a short flight-time and therefore may still be partly fluid when they land, but because the fountains are short-lived they do not accumulate fast enough to completely coalesce, therefore forming spatter and scoria deposits. In more energetic events, sometimes referred to as "violent Strombolian," eruption columns may have a substantial buoyant plume component that carries smaller scoria clasts and ash to altitudes of hundreds or thousands of meters (Figure 3). The clasts then rain out, blanketing the landscape as well-sorted fallout deposits. These eruptions then begin the transition to larger sub-Plinian and Plinian events described below.

Vulcanian eruption columns are commonly caused by exploding hydrothermal systems within volcanic vents, where magmatic gases and/or meteoric steam accumulates beneath a hot, partially- or completely-solidified magma plug, until sufficient pressure builds up to blow part of the plug out in discrete explosions. These eruptions often have a large proportion of fine ash, so that while large clasts follow a ballistic path or a fountain-like path, fine ash is lofted to hundreds or thousands of meters altitude. Small scale explosions of this type are quite common at active composite cones (Figure 4). Other types of hydrovolcanic eruptions (e.g., those termed *Surtseyan* in some of the literature) can produce discrete or sustained explosions that send fine ash up to 10 km and sometimes greater altitudes.

Sustained, powerful eruptions, mainly of intermediate to silicic composition, form the *Plinian* spectrum of eruption columns. When conditions are such that the columns become buoyant relative to the atmosphere, they (the columns) can rise to altitudes of 20 km (subplinian) to as high as 50 km (ultraplinian) producing widespread pumice fallout deposits. When these eruptions form fountaining (collapsing) columns, the particle-gas mixture flows radially outward as pyroclastic flows. The most impressive of these eruptions are associated with huge calderas, where multiple vents with a variety of geometries may produce several simultaneous eruption columns.

In this paper I focus mainly on the fluid dynamics of large-scale eruption columns. The dynamics of these columns are rooted in multiphase flow phenomena, so a major part of the paper sets up a foundation on that topic that allows one to quickly assess the inherent assumptions made in various theoretical and experimental approaches. This first part is centered on a set of complex differential equations that describe eruption columns, but the focus is on a general understanding of important physical processes rather than on the mathematics. I discuss briefly the relative merits and weaknesses of different approaches, emphasizing that the largest advances in understanding are made by combining them. I then focus on dynamics of steady eruption columns and then on transient phenomena. Finally I briefly review the effects of varying behavior of the ambient medium through which an eruption column moves. These final sections will emphasize concepts and a qualitative understanding of eruption dynamics. This paper relies on principles of continuum mechanics and transport processes but does not go into detail on the development of those principles. For a more general introduction to continuum mechanics in the earth sciences I recommend the books by Middleton and Wilcock (1994) and by Turcotte and Schubert (1982). An excellent resource on transport processes in multiphase and multicomponent systems, with lucid explanations of conservation equations, is the book by Bird et al. (1960).

2. Multiphase flow and the multifield approach

The term *multiphase* flow refers to flows with some combination of vapor, liquid, and solid. Eruption columns typically have all three of these. The vapor or gas phase consists of magmatic gases, steam from groundwater or surface water, and entrained air. Liquid is present in the form of clots or

droplets of melt and as water droplets. Solids include quenched magma fragments (e.g. glass shards and pumice), lithic debris entrained from the vent walls, and ice crystals as a column rises to high altitudes. Each different type of material within a given phase (e.g. steam and air in the vapor phase) is a different component; therefore eruption columns not only are multiphase, but are *multicomponent* flows as well.

Each of the material phases in an eruption column must conserve mass, momentum, and energy (Figure 5). In multiphase flows where the phases are dispersed amongst each other, such as in an eruption column, we can use the *multifield* approach to describing the flow and interaction of the phases. A first step in developing conservation equations for fluid flow problems is to designate a control volume, or representative elementary volume (REV), as shown in Figure 5. The REV is smaller than the scale of important dynamics in the system, but large enough that the fluid can be treated as a continuum. In the multifield approach for explosive eruptions the REV must contain a large enough number of solid particles or liquid drops that they can be treated as continua rather than as discrete particles or drops (Figure 6). An REV in a such a multiphase system is then occupied by a combination of gas, solid and liquid continua, each in proportion to their volume fractions (which sum to unity). This will become clear in the governing equations presented below.

A fundamental issue in eruption column physics is not just the existence of muliple phases within the REV, but the interaction between them. These interactions occur through exchange of mass, momentum, and energy. Mass is exchanged, for example, as gas diffuses from clasts (solid-gas coupling), and as water droplets condense from vapor (liquid-vapor coupling). Drag between clasts and the surrounding gas results in momentum exchange between phases. Energy is exchanged by heat transfer (for example hot clasts heating surrounding gas), by drag that causes viscous dissipation, and by exchange of latent heats during phase changes. All of these are discussed in some detail throughout this paper.

3. Multifield governing equations

Valentine (1994) proposed a multifield framework for magma dynamics ranging from melting in the mantle to magma chamber processes and ultimately to eruption. In this paper I use the subset of those equations, with some modifications, that hold when the gas phase is continuous (incompressible solid

particles and liquid drops dispersed within the compressible gas), as is the case with all explosive eruption columns. Table 1 defines all symbols.

3.1 Conservation of mass

Conservation of mass for the gas is

$$\frac{\partial(\theta_v \rho_v)}{\partial t} + \nabla\cdot(\theta_v \rho_v \boldsymbol{u}_v) = \sum_{r=1}^{q} \Gamma_r \quad . \qquad (1)$$

The first term in equation 1 is the rate of change of gas contained within an REV, while the second term is the change in gas flux into and out of the REV. The Γ terms account for vapor exsolution and evaporation (positive Γ; negative Γ if dissolution or condensation) from each of the q particle and droplet populations, and will be discussed in a subsequent section. The gas phase in an eruption column consists of two major components, water vapor and air. The different thermodynamic properties of these two components are responsible for important aspects of eruption dynamics, as will be seen below. Thus we track the two components with additional conservation equations (Dobran et al., 1993). For air,

$$\frac{\partial(\theta_v \rho_v y_a)}{\partial t} + \nabla\cdot(\theta_v \rho_v y_a \boldsymbol{u}_v) = 0 \quad , \qquad (2)$$

where y_a is the mass fraction of air. For water vapor,

$$\frac{\partial(\theta_v \rho_v y_w)}{\partial t} + \nabla\cdot(\theta_v \rho_v y_w \boldsymbol{u}_v) = \sum_{r=1}^{q} \Gamma_r \quad , \qquad (3)$$

where y_w is the mass fraction of steam. Note that exsolution/dissolution only affects water vapor since it is a magmatic volatile and air is not.

Conservation of mass for the dispersed, incompressible particles and liquid drops is expressed by a family of equations. Each equation in this family conserves a specific population of particles or drops.

A population is defined as a discrete size and density range (for example, one might define a population of pumice clasts between 1-2 cm diameter, another population of dense lithic clasts 1-2 cm diameter, and so on). The equations are:

$$\begin{aligned} \frac{\partial(\theta_p\rho_p)_1}{\partial t} + \nabla\cdot(\theta_p\rho_p u_p)_1 &= -\Gamma_1 + \sum_{r=1}^{q} \delta_{1r}Q_{1r} \\ &\vdots \\ \frac{\partial(\theta_p\rho_p)_q}{\partial t} + \nabla\cdot(\theta_p\rho_p u_p)_q &= -\Gamma_q + \sum_{r=1}^{q} \delta_{qr}Q_{qr} \end{aligned} \quad , \quad (4)$$

where

$$\begin{aligned} \delta_{qr} &= 0 \quad \text{if } r=j \\ \delta_{qr} &= +1 \quad \text{if } r\neq j \end{aligned} \quad . \quad (5)$$

The Q terms account for addition of mass to a population from other populations. For example, large pyroclasts can generate ash size particles as a result of abrasion, or water droplets might grow in diameter.

Note that the volume fractions must sum to unity:

$$\theta_v + \sum_{r=1}^{q} (\theta_p)_r = 1 \quad . \quad (6)$$

3.2 Conservation of momentum

Momentum conservation for the gas is expressed as

$$\begin{aligned} \frac{\partial(\theta_v\rho_v u_v)}{\partial t} + \nabla\cdot(\theta_v\rho_v u_v u_v) = &- \theta_v\nabla p_v + \sum_{r=1}^{q} \Gamma_r u_{pr} \\ &- \sum_{r=1}^{q} (K_v\Delta u_v)_r + \theta_v\rho_v g - \nabla\cdot(\theta_v\tau_v) \end{aligned} \quad (7)$$

The first term in Equation 7 is the rate of change of momentum within an REV, and the second term is momentum advected out minus that advected into the the REV. The third term, on the right hand side of the equation, is momentum due to pressure gradients. The fourth term is momentum of vapor being added or subtracted to the gas phase from populations of the solid or liquid phases; for example, as vapor leaves a shrinking water drop it initially has the velocity of the drop, rather than the surrounding gas. The fifth term is the drag force summed over the particle and drop populations. This is proportional to the velocity difference between the phases, $\Delta u_{vr} = u_v - u_{pr}$. The sixth term is the downward force due to gravitational acceleration, and the final term is momentum transport by viscous forces (as will be seen below this is effectively dominated by turbulence). The terms on the right hand side require equations of state and constitutive equations, which will be discussed below.

The momentum equations for the particles and drops are

$$\begin{aligned}
\frac{\partial(\theta_p\rho_p u_p)_1}{\partial t} + \nabla\cdot(\theta_p\rho_p u_p u_p)_1 &= -\theta_{p1}\nabla p_p - \Gamma_1 u_{p1} + \sum_{r=1}^{q}\delta_{1r}(Q_{1r}u_{pr} + K_{1r}\Delta u_{1r}) \\
&\quad + (K_v\Delta u_v)_1 + (\theta_p\rho_p g)_1 - \nabla\cdot(\theta_{p1}\tau_p) \\
&\vdots \\
\frac{\partial(\theta_p\rho_p u_p)_q}{\partial t} + \nabla\cdot(\theta_p\rho_p u_p u_p)_q &= -\theta_{pq}\nabla p_p - \Gamma_q u_{pq} + \sum_{r=1}^{q}\delta_{qr}(Q_{qr}u_{qr} + K_{qr}\Delta u_{qr}) \\
&\quad + (K_v\Delta u_v)_q + (\theta_p\rho_p g)_q - \nabla\cdot(\theta_{pq}\tau_p)
\end{aligned} \tag{8}$$

The terms on the right hand side of each equation in this set represent: the pressure gradient in the pyroclast field (only applicable at high concentrations) multiplied by the volume fraction of a specific population; the velocity of vapor being lost or added from the particles and drops, momentum brought into the population from other populations (e.g., a fragments of a just-broken clast will initially have the velocity of their parent) and drag between populations (determined by the slip velocity $\Delta u_{qr} = u_r - u_q$), interfacial drag, gravitational acceleration, and the viscous stress in the pyroclast field (only applicable at high concentrations). An example of the use of pressure in the pyroclast field can be found in Dobran et al. (1993), and will be discussed below.

3.3 Conservation of specific internal energy

Conservation of specific internal energy (internal energy per unit mass) for the vapor phase is written as

$$\frac{\partial(\theta_v\rho_v I_v)}{\partial t} + \nabla\cdot(\theta_v\rho_v I_v \boldsymbol{u}_v) = p_v\nabla\cdot(\theta_v\boldsymbol{u}_v) + \nabla\cdot(\theta_v k_v\nabla T_v) + \sum_{r=1}^{q}(F + K_v|\Delta u_v|^2 + R_p\Delta T_p)_r \quad + \quad \theta_v\tau_v:\nabla\boldsymbol{u}_v \tag{9}$$

where the first term on the right hand side is work, and the second is heat conduction through the gas. The third term is the sum of latent heat from phase change, viscous dissipation due to interphase drag, and heat transfer between phases ($\Delta T_{pr} = T_{pr}$-T_v), summed over all the particle and drop populations. The final term is viscous dissipation.

Specific internal energy conservation for the particle and drop fields is written as

$$\begin{aligned}
&\frac{\partial(\theta_p\rho_p I_p)_1}{\partial t} + \nabla\cdot(\theta_p\rho_p I_p\boldsymbol{u}_p)_1 = \nabla\cdot(\theta_p k_p\nabla T_p)_1 - (R_p\Delta T_p)_1 + (\theta_p\tau_p:\nabla\boldsymbol{u}_p)_1 \\
&\qquad\qquad\qquad\qquad\qquad\qquad\qquad\qquad\qquad\qquad\qquad\qquad\qquad\qquad\qquad\qquad\qquad\qquad \vdots \qquad\qquad\qquad\qquad\qquad\qquad\qquad\qquad\qquad\qquad\qquad\qquad\qquad\qquad\qquad\qquad\qquad\qquad (10) \\
&\frac{\partial(\theta_p\rho_p I_p)_q}{\partial t} + \nabla\cdot(\theta_p\rho_p I_p\boldsymbol{u}_p)_q = \nabla\cdot(\theta_p k_p\nabla T_p)_q - (R_p\Delta T_p)_q + (\theta_p\tau_p:\nabla\boldsymbol{u}_p)_q
\end{aligned}$$

The right hand side of equations (16) include heat conduction, interphase heat transfer, and viscous dissipation terms. The heat conduction and viscous terms only become important when pyroclasts are present in high enough concentrations that they are in nearly constant contact. For example, the conductive term is important for freshly-deposited ignimbrite (e.g., Riehle, 1973). The viscous term will be important during final high-concentration movement of pyroclastic flows, in which case it will reflect the properties of a granular mixture.

4. Closure of governing equations

The number of partial differential governing equations (equations 1-10) is smaller than the number of variables in the system. This requires another set of equations to close the system so that it can be solved. These closure equations fall into four categories. (1) *Equations of state* describe the relationships between the thermodynamic properties (temperature, specific internal energy, density, and pressure) for each material field in the governing equations. (2) Constitutive equations describe the response of one of the material fields to applied forces. (3) *Interphase exchange relationships* define how mass, momentum, and energy can be exchanged between the material fields or phases. (4) The final category is *material properties* such as thermal conductivity and heat capacity. The necessary relationships within each of these categories are discussed below.

4.1 Equations of state

For eruption columns it is sufficient to use an ideal gas equation of state for the vapor phase. Following Dobran et al. (1993), who applied simple mixture theory to account for the vapor phase being a combination of air and water vapor,

$$P_v = \rho_v R_m T \quad , \tag{11}$$

where the gas constant for the mixture, R_m, is determined by the mole fractions, x_w and x_a, of water vapor and air, respectively and the molecular weights of water vapor and air (M_w, M_a):

$$R_m = \frac{\overline{R}}{x_w M_w + x_a M_a} \quad . \tag{12}$$

Here $\overline{R}$ is the universal gas constant. The mole fractions can be determined from the mass fractions by

$$x_n = \frac{y_n}{M_n} \frac{1}{\frac{y_w}{M_w} + \frac{y_a}{M_a}} \quad , \quad n = w,a \quad . \tag{13}$$

The temperature of the vapor phase is related to the specific internal energy by

$$I_v = c_{vv} T_v \quad , \tag{14}$$

where the specific heat at constant volume for the vapor mixture (c_{vv}) is

$$c_{vv} = x_a c_{va} + x_w c_{vw} \quad . \tag{15}$$

The particle/drop field is assumed to be composed of incompressible solids or liquid water. Therefore the only necessary state equation for a given population, r, within that field is

$$I_{pr} = (c_{vp})_r T_{pr} \quad , \tag{16}$$

$(c_{vp})_r$ being the specific heat for the given population (e.g., juvenile clast, lithic clast, or liquid water).

4.2 Constitutive equations

Within the context of the governing conservation equations (1-10), constitutive equations include viscous and turbulent momentum transfer, and granular "pressure" in the solids field when concentrations become sufficiently high. For the vapor phase, the stress tensor is (Dobran et al., 1993)

$$\tau = \mu_v \left[\nabla \boldsymbol{u}_g + (\nabla \boldsymbol{u}_g)^T - \frac{2}{3} (\nabla \cdot \boldsymbol{u}_v) \boldsymbol{I} \right] \quad , \tag{17}$$

where the viscosity (μ_v) in a strict sense is the sum of the molecular viscosity of the vapor and the turbulent "viscosity." The latter is orders of magnitude larger than the former in eruption columns, which are highly turbulent, therefore we only consider turblence effects. Turbulence, through the action of eddies, efficiently transports momentum both transverse to and along the axis of mean flow in eruption

columns, and this is captured in equation 17 (note, superscript T is the transpose operation, and $\boldsymbol{I}$ is the unit tensor). The simplest model of turbulent momentum transfer is a mixing length approach, where the "turbulent" vapor phase viscosity is simply a length scale multiplied by the local velocity gradient. The length scale is chosen to represent the size of the dominant momentum-transporting eddies in the flow. More sophisticated treatments of turbulence exist, but are not as well understood for multiphase systems such as eruption columns as they are for single fluid systems.

The stress tensor for the incompressible particle and drop fields is more difficult. The most thorough treatment to date is that of Dobran et al. (1993), who used a kinetic theory of granular flow; clearly this pertains only to populations of solid particles in the eruption column, and not liquid drop populations. In the kinetic theory approach the pressure of the solid particle fields is due to random motion of particles and collisions with other particles. It is a complicated function of particle concentration, size, elastic properties, shapes, and velocity gradients. The modeling of Dobran et al. (1993) and subsequent applications of that model have included pyroclastic flow processes, where particle concentrations become relatively high (greater than approximately 0.1) and particle-particle interactions are therefore important. However, in eruption columns the particle concentrations are typically much lower, $<10^{-2}$, so that particle-particle interactions are unimportant and the pressure of the incompressible fields can be ignored. A topic of important research in the future will be to develop rigorous constitutive equations for the incompressible particle and drop fields in a way that can be used with the population approach of equations 1-10. This will be a necessary step for addressing flow and deposition mechanics for pyroclastic flows and surges.

4.3 Interphase exchange relationships

In the governing equations described above there are several important terms that describe exchange of mass, momentum, and energy between phases. Probably the most important of these, in terms of their effects on large-scale dynamics of eruption columns, are momentum (drag) and heat exchange between the vapor and particle/drop fields. Here I give examples of these relationships from the most recent literature on multiphase eruption modeling. Before conducting one's own analysis, it is

important to carefully assess these relationships and to understand the simplifications implied by them. Depending on the goal of one's analysis, other relationships may be more suitable.

The mass conservation equations (1-4) contain two types of interphase transfer, condensation of water vapor to liquid drops (Γ-terms) and terms that describe the growth or decay of particles and drops from one population to the next (Q-terms). These transfer terms would benefit from further research. Condensation effects have been treated in two ways. First, Woods (1993a,b) assumed that condensation in eruption columns is essentially an instantaneous process, due to the abundance of ash particles that serve as nuclei. This approach assumes that parcels of eruptive mixture (plus entrained air) contain sufficient liquid water to keep the mixture just at the saturation pressure for the local temperature, thus determining the volume fraction of drops. Glaze and Baloga (1996) consider the effect of the condensation rate (as opposed to instantaneous condensation) on column dynamics. However, no work to date has considered the size distribution and growth/decay of drops in eruption columns; it is likely that much could be learned along these lines from the meteorological literature (specifically that pertaining to thunderstorms). Similarly, the Q-terms that also describe the growth or decay of particles from one population to the next (e.g., growth of accretionary lapilli, or breakage of pumice clasts, respectively) have not been quantified to date.

Momentum transfer between a particle or drop population, r, and the surrounding vapor depends on a drag function $(K_v)_r$, which we adopt from Wallis (1969) and Dobran et al. (1993):

$$(K_v)_r = \frac{3}{4}\theta_v^{-2.7} C_{dr} \frac{\theta_v \theta_{pr} \rho_v |\boldsymbol{u}_v - \boldsymbol{u}_{pr}|}{d_{pr}} \quad , \tag{18}$$

where d_{pr} is the diameter of the particles or drops in the population. C_d, the drag coefficient, depends on the particle Reynolds number (Re_{pr}); at low Re_{pr}, fluid flow around a particle/drop is dominantly laminar, while at greate values it is turbulent.

$$C_{dr} = \frac{24}{\theta_v Re_{pr}}\left[1 + 0.15(\theta_v Re_{pr})^{0.687}\right] \qquad \theta_v Re_{pr} < 1000 \quad , \tag{19}$$

$$C_{dr} = 0.44 \qquad \theta_v Re_{pr} \geq 1000 \quad , \tag{20}$$

with

$$Re_{pr} = \frac{\rho_v d_{pr} |u_v - u_{pr}|}{\mu_v} . \tag{21}$$

In this discussion I have ignored the momentum exchange between different populations (the drag of one population on another); Neri and Macedonio (1996) discuss this issue for problems with two particle sizes, as reviewed below, and it appears that this is a topic that would benefit from further theoretical and experimental research. It is likely to be important in pyroclastic flows, but in eruption columns, outside the regime of more concentrated pyroclastic flows, this coupling is probably of minor importance.

Heat transfer from particles and drops to the vapor phase, and vice versa, depends on several processes. Heat is exchanged from the surface of a particle or drop by a combination of conduction into the vapor, forced convection due to the slip velocity $|u_v - u_{pr}|$, and radiative transport (proportional to T^4). The heat supplied to the surface of a particle or drop from its interior is limited by conduction (particles) or internal circulation (drops). This can be quantified with the Biot number, which is the heat transfer rate from individual particles/drops to the surrounding vapor divided by their internal heat transfer rate. For large clasts, this internal heat transfer needs to be accounted for. However, for sufficiently small particles (ash) or droplets, where the Biot number is much less than unity, this is a negligible effect. An example of interphase heat transfer for ash size particles is the set of relations used by Dobran et al. (1993):

$$R_{pr} = Nu_r \frac{6 k_v \theta_{pr}}{d_{pr}^2} \quad , \tag{22}$$

$$\mathrm{Nu_r} = (2 + 0.16 Re_{pr}^{0.67}) \qquad Re_{pr} \leq 200 \quad , \tag{23}$$

$$Nu_r = 8.2 Re_{pr}^{0.6} \qquad 200 < Re_{pr} \leq 1000 \quad , \tag{24}$$

$$Nu_r = 1.06 Re_{pr}^{0.457} \qquad Re_{pr} > 1000 \quad . \qquad (25)$$

Note that these are empirically derived equations, and reflect primarily the importance of the boundary layer around the particle or drop. The structure of the boundary layer depends on Re_{pr}, the particle Reynolds number, which determines whether the flow in the boundary layer is laminar or turbulent, and to what degree it is turbulent. Equations 22-25 account only for the forced convective heat transfer component, which in most types of eruptions probably dominates over conductive and radiative transfer.

4.4 Material properties

Finally, several material properties are required to close the system of governing equations. First among these are densities of the incompressible phases (particles and liquid drops), ρ_{pr}, which can be different among populations (r). For example one might define two populations that include particles between 1-2 cm diameter, where one population is dense lithic clasts and the other is low-density pumice clasts. Also, of course, water drops will have a different material density than many clasts of the same size. Thermal conductivities and heat capacities for the phases also must be specified. Dobran et al. (1993) provide values for these properties that can serve as a starting point for further studies.

5. Approaches to analysis of eruption column dynamics

There are three main approaches that can be taken to studying eruption column dynamics within the context of the governing equations (1-10) given above: (1) experimental approaches, (2) theoretical studies that simplify the governing equations so that analytical or semi-analytical solutions may be found, and (3) direct numerical solution of the equation set. Each one of these has its strengths and weaknesses, but they are complimentary and it is necessary to pursue all three approaches. I am setting aside observational approaches in this paper -- these are always indirect due to the extreme conditions and unpredictibility of eruption columns, and will be covered in the paper on fallout deposits by M. Rosi.

Many fluid dynamics problems can be simulated by scaled laboratory experiments. For example, most early designs of high-speed aircraft, rocket nozzles, and water-works were based on scaled experiments. Scaling is done by means of dimensional analysis which reduces the primitive variables of a system to a smaller set of dimensionless parameters. An excellent description of dimensional analysis is provided by Li and Lam (1964). Middleton and Wilcock (1994) also describe the method, and go into some detail on its application to earth science problems. The combination of compressible flow (high Mach number), turbulence (high Reynolds number), gravitational influence, and multiphase processes make it difficult to produce true scaled models of eruption columns. However, individual aspects of the dynamics can be abstracted and scaled for experiments; examples that will be discussed in this paper include the work of Kieffer and Sturtevant (1984), Anilkumar et al. (1993), and, briefly, Erst et al. (1994). It is essential to keep in mind that such experiments only look at specific aspects of eruption columns, though, and necessarily exclude other processes that may be strongly coupled. Quantitative empirical relationships derived from such experiments should only be applied to natural eruptions with extreme caution.

Analytical or semi-analytical theoretical approaches seek exact solution of the governing equations. These require significant simplification of the governing equations as I present them in this paper, and can only look at subsets of eruption column behavior. Typical simplifications include: steady flow in eruption columns (no time dependence), single phase flow (which implicitely assumes perfect mass, momentum, and energy coupling between particles, drops, and vapor), and incompressible flow. Even with such simplifications the dynamics are quite rich and difficult to quantify. This approach is necessary for isolating some aspects of eruption column dynamics for understanding. Examples to be discussed in this paper are Woods (1988), Wilson et al. (1978), Glaze and Baloga (1996), and Glaze et al. (in press). These approaches require similar caution in their application to natural eruptions as the experimental approaches described above -- typically the authors are quite clear about the bounds within which their theories apply.

Direct numerical simulation of the governing equations uses finite difference or finite element approximations of the differential equations 1-10, or a subset of them. This approach is promising in that

it allows us to relax some of the simplifications in the physics that must be made in the approaches described above. Its drawbacks lie in the necessary initial investments of computer programming and in hardware (note that much can be done nowadays with relatively inexpensive workstations, rather than mainframe computers), in the difficulties in validating the numerical solution techniques, and in the difficulties in obtaining accurate constitutive equations to close the governing equations. Many of these drawbacks can be addressed by using analytical and experimental approaches, for example, to validate aspects of the numerical models and to obtain constitutive equations. In this paper I will review results of numerical simulation studies by Valentine et al. (1991, 1992), Dobran et al. (1993), Neri and Dobran (1994), and Neri and Macedonio (1996).

6. Steady state dynamics

Much of our understanding of eruption columns is based on theory that has been developed for steady state conditions, where there is no temporal variation in the eruption column. In equations 1-10, this means that the $\partial/\partial t$ -terms, on the left hand sides of the equations, are dropped. In the steady state theories the flows are considered to be one-dimensional, along the vertical axis only. Particles and drops are considered to be perfectly coupled to the gas, that is, they move with the same velocity and have the same temperature as the gas. This effectively assumes that the dynamics are dominated by very fine ash. The eruption column then is treated as a "pseudogas," with density and thermal properties determined by the mixture of vapor and particles/drops. These simplifications reduce equations 1-10 to a set of three steady state equations, conserving mass, vertical momentum, and energy for the pseudogas. It is important to consider the importance of these simplifications, which, while "liberating" in the sense that they allow one to use relatively straightforward mathematics, are "restrictive" in the sense that they eliminate a wide range of processes that can have first-order effects on the eruptions.

Before entering into a discussion of eruption column behavior, it is important to review the range of flow parameters as the eruptive mixture exits the vent since these form the boundary and initial conditions for the eruption columns. Vent exit conditions are determined by the rise of magma from its reservoir. The paper by Dingwell in this volume discusses in detail what is known about the process of

magma fragmentation. There have been two basic approaches to determining the continued acceleration and decompression of the eruptive mixture above the fragmentation surface. One of these, developed initially by Wilson et al (1980), assumes that as the mixture rises it maintains a pressure distribution that is very close to the lithostatic pressure gradient in the adjecent country rock (note - Wilson et al. also considered cases with different assumptions about pressure, but the discussion here focuses on the approach that they adopted for most eruption column calculations). This assumption in turn implies that the conduit walls are very weak and that any local change in flow pressure relative to lithostatic pressure is immediately accomodated by wall failure. Flow is assumed to be isothermal in the conduit, with particles and gas having the same temperatures and velocities so that the mixture is treated as a single phase psuedogas. In this case, for a given mass flux, the mixture velocity and the conduit shape can be calculated. This approach results in conduits that flare at shallow depths and in jets that exit the ground as "pressure balanced jets," that is, they exit at atmospheric pressure. For a given mass flux and volatile content of magma flowing into the base of the conduit, exit velocity, vent radius, mixture density (from which particle concentration can be computed). The Wilson et al. (1980) approach has been the most widely used one for determining exit conditions. A second approach is that of Dobran (1992), Macedonio et al. (1994) and coworkers. This approach assumes that the conduit size is constant in its vertical dimensions and that the flow is isothermal, but does not assume that the particles and gas have the same velocity. For a given mass flux the pressure and velocity distribution can be calculated, and the exit pressure is commonly larger than atmospheric. Both of the above approaches to computing vent exit conditions assume steady state flow, and they yield exit velocities of 100-600 m/s, exit pressures from 0.1-30 Mpa, and vent diameters from 5 m to hundreds of m. While both approaches provide combinations of parameters such as velocity, particle concentration, pressure, and vent radius for the idealized one-dimensional conduit geometries they assume, we need to keep in mind that natural eruptions can be quite "messy," espcially for larger events that induce caldera collapse. Many vents may discharge magma simultaneously, and each vent may have its own size and geometry. Introduction of groundwater and wall-rock debris can further complicate the vent parameters for an eruption column.

6.1 Entrainment

An important fluid dynamic process in eruption columns is *entrainment.* Eruptive mixtures are expelled from the vent at high velocities and are turbulent. As the column enters the atmosphere there is a great deal of shear between its margins and the surrounding atmosphere. The margins are unstable and vortices form. The swirling motion of the vorticies enfolds air into the column, distorting each "parcel" as it entangles with subsequent vortices and smaller eddies, and the air continues to mix toward the interior of the column as it is carried vertically with the mean flow. This process of enfolding and mixing of air into the column is called entrainment; Brown and Roshko (1974) provide an excellent description of the dynamics of this process. Entrainment is most effective when the two fluids (the flowing fluid and the ambient fluid) have similar densities and viscosities and when the flow speeds are in the incompressible range (Figure 7). For eruption columns, particularly in the jet region, the density ratio between the column and the atmosphere and Mach number can both be quite high. Woods (1988) has accounted for the density ratio effects in his eruption column theory. However, I am not aware of any work that has incorporated Mach number effects on entrainment in eruption columns.

6.2 Buoyant vs. collapsing columns

The opening paragraph of this paper provides a conceptual description of the basic parts, driving forces, and behaviors of eruption columns. The two parts of an eruption column are the jet or "gas thrust" region, and the buoyancy driven region (Figure 1). In the jet region at the base of a column, the mixture is denser than the atmosphere and is driven upward by its initial kinetic energy as it leaves the vent and by continued expansion of the gas until it equilibrates with atmospheric pressure. In the buoyancy driven region, the mixture continues to flow upward because it is less dense than the surrounding atmosphere. There are two basic behaviors of eruption columns - buoyant columns and collapsing columns (also referred to here as fountains).

A great deal of work has been done on the combinations of eruption parameters, under steady state conditions, that will determine whether a column becomes buoyant or collapses. As stated in the Introduction, all explosive eruption mixtures exit the vent denser than the atmosphere. For a column to

become buoyant it must entrain and heat sufficient air so that the mixture of particles, volcanic gases, and air becomes less dense than the atmosphere, before the mixture reaches the height at which the initial kinetic energy of the jet has been spent. Development of buoyant columns is favored by the following conditions: (1) narrow vents (and therefore narrow columns), so that a relatively large surface area for entrainment is present on the column margins compared to the volume of material in the plumes (note that the area along the column margins available for entrainment increases as radius squared, but the volume of material within the column that needs to be mixed with air increases as radius cubed); (2) high exit velocities which strengthen the entrainment process and give entrainment a larger height over which to act before initial kinetic energy is spent; (3)high gas contents at the vent, which reduce the initial density of the mixture. Valentine and Wohletz (1989) also suggest that a high pressure ratio at the vent also promotes development of buoyant columns, although more numerical work needs to be done to confirm this.

Figure 8 illustrates these dependencies within the context of a one-dimensional, steady-state, psuedogas model developed by Woods (1988). In Figure 8a, the dashed line represents the critical conditions for column collapse (to the left of the dashed line, all columns collapse, while to the right all become bouyant) for eruptions from a 100 m radius vent. The solid curves show the height of the top of bouyant columns as a function of exit velocity, for gas (H_2O) mass fractions of 5, 3, 1, and 0.5%. The dashed curve shows that for slightly increasing exit velocity (from about 70-100 m/s) the gas fraction must decrease drastically, by a factor of ten, in order to maintain column collapse conditions. Another interpretation would be that if a zoned magma were erupting at a constant speed of 100 m/s from a 100 m radius vent, its volatile content would have decrease from several weight percent to about 0.5% H_2O to go from a buoyant to a collapsing column.

Figure 8b shows the height of the jet or gas thrust part of the column, again for vent radius of 100 m, as a function of exit velocity for different gas contents. Note that the gas thrust part is where the column is denser that the atmosphere and is therefore driven upward by its initial kinetic energy. The dashed lines show this relationship where the column collapses at the top of the gas thrust region, in other words it is unable to attain buoyancy. The Figure shows that the collapse height is very sensitive to exit velocity, which is expected since the initial kinetic energy is proportional to velocity squared.

Interestingly, for columns that become buoyant (solid parts of curves) the height of the gas thrust region decreases with increasing velocity owing to the increased efficiency of entrainment at higher velocities. An example of what this plot would indicate for a real eruption from a 100 m radius vent is that for a constant gas content of 3% in the erupting magma, at initial velocities of say 200 m/s the column would be bouyant (producing fallout deposits). As its exit velocity waned with time the column would begin collapsing (producing pyroclastic flows and surges) when the exit velocity reached about 80 m/s, and the fountain height would be about 750 m above the vent. Continued decrease in exit velocity would cause drastic drops in the fountain height, which may be reflected as progressively less mobile pyroclastic flows through time. Note that these changes would have to occur very slowly for the steady state theory to remain approximately correct.

Figure 8c shows column height as a function of vent radius, for several combinations of eruption temperature and gas content. Following one of the curves, starting at a vent radius of 10 m, we see that for the cases shown the columns are buoyant. They then rise to an altitude where the atmospheric density and column density are equal (neutral buoyancy). Were the vent to gradually widen due to erosion during the eruption, the plumes initially grow in height as more and more potential for buoyancy is added to the system in the form of hot ash and gas. However, each column eventually reaches a point where the column is too wide for sufficient air to be entrained to attain buoyancy. At this point the column collapses and forms a fountain that is typically a few hundred meters to a kilometer high.

These examples serve to illustrate the dependence of column behavior on gas content, vent radius, and exit velocity. Woods and Bursik (1991) extended the above models to account for thermal disequilibrium between particles and gas such as would occur when a large fraction of the particles are larger than several millimeters in diameter. They found that such disequilibrium could have a very strong influence on whether a column will collapse or become buoyant; columns where there is a high degree of disequilibrium are less likely to become buoyant because many of the particles, which supply heat for buoyancy, retain their heat and fall out of the column. Figure 9 illustrates this effect.

6.3 Supersonic dynamics and role of pressure in the jet region

I have alluded to the fact that most eruptive mixtures exit the vent at supersonic speeds during explosive eruptions. The speeds themselves are high (10s to 100s of m/s), but what determines whether the flow is supersonic is the ratio of the flow speed to the sound speed in the mixture, or the Mach number. If the Mach number is greater than one, the flow is supersonic and this means that pressure waves can only propagate in the direction of flow. A result of this is formation of shocks and other complexities if the flow is trying to equilibrate with the ambient fluid. Eruptive mixtures of gas and particles have lower sound speeds than clean gas, as low as a few tens of m/s (Figure 10). This is related to the relatively high heat capacity of the mixture,which results from the presence of particles, and the effect of particles on the mixture density relative to the mixture's compressibility, which is due mainly to the gas. I will not go into further detail on compressible flow processes here beyond describing effects on eruption column processes; the general processes will be covered in more detail in the paper by Wohletz in this volume.

Eruption columns widen with increasing altitude for two main reasons: entrainment and equilibration with atmospheric pressure. If an eruption column exits the vent with a pressure equal to the atmospheric pressure, it is called a "pressure-balanced" jet. Under steady state conditions, a pressure-balanced jet will gradually widen with increasing altitude. The primary reason for this is entrainment -- as more air is incorporated into the column it becomes less dense and occupies a greater volume. Entrainment is sensitive to flow velocity and the density ratio between the column and the atmosphere; the spreading angle is quite high (c. 20° outward from the vertical around the edges of the column) near the base of the column due to the high velocities there (Woods, 1988).

Eruption columns that exit the vent at pressures exceeding atmospheric pressure, and at supersonic speeds, are called "overpressured jets" (or "underexpanded jets;" Kieffer and Sturtevant, 1984). Overpressured jets widen upwards due to entrainment as described above, but they also widen as the flow expands to equilibrate with the atmosphere. Figure 11 illustrates the manner in which an overpressured jet equilibrates with atmospheric pressure. As the jet exits the vent, it immediately begins to expand through a "fan" of expansion (rarefaction) waves. These waves are attached to the rim of the vent and the propagate

upward and outward to form a rarefaction fan (note that the expansion waves cannot propagate back into the conduit because the flow is supersonic). The erupting mixture expands, accelerates, and is diverted outward through these waves, producing a flaring shape at the base of the column. This outward flaring is stronger at higher jet pressures and may reach values as high as c. 45° outward on either side of the column (Kieffer and Sturtevant, 1984). Just downstream from the vent, the core of the accelerating jet may overcompensate and attain pressures less than the atmosphere. Meanwhile, the expansion waves in the rarefaction fan intersect the edge of the jet and are reflected back inward as compression waves. Further downstream these compression waves join to form a shock wave that pulls the flow radially inward. The shock waves on either side of the jet eventually join downstream in the center of the jet to form a strong, stationary shock (referred to as a Mach disk shock in Figure 11). As fluid in the core of the jet passes through this shock it decelerates and is recompressed to a pressure between the vent pressure and the atmospheric pressure. Depending on the degree of overpressure one Mach disk shock may be sufficient to attain equlibrium with atmospheric pressure, or repeated patterns of expansion followed by Mach disk shock may be necessary.

Figure 12 shows an experiment by Kieffer and Sturtevant (1984) that simulates some of the compressible flow effets expected in eruption columns. These small-scale experiments discharged gas from a high pressure reservoir (beneath what is shown in the photographs) into a low pressure "atmosphere." The gases were selected to have similar thermodynamic properties to eruptive mixtures within a pseudogas approximation. The shades of grey in the photographs record the density of the gas -- high densities are brighter. The "vent" from which the jet flows is 1.5 cm in diamter, and this provides a scale. The top photo is at an early time (500 μs after flow initiation), and shows the vortex structure at the top of the jet and the development of a single Mach disk shock system just above the vent. The lower photograph shows the jet at a later time (2.25 ms) when steady flow conditions have been established, and several Mach disk shocks can be seen, each bringing the flow progressively closer to the atmospheric pressure. In natural eruption columns we do not know how important these processes are because the interiors of the columns are obscured by ash. However, we suspect that overpressured eruptions do occur

-- the 18 May 1980 blast at Mount St. Helens was probably just such a jet, but it was discharged laterally across the ground rather than vertically (Kieffer, 1981).

6.4 Buoyant eruption column height

A buoyant eruption column will rise until its density equals the local atmospheric density. This is complicated in nature because the temperature structure of the atmosphere is such that, moving upward from the ground, the temperature initially decreases with altitude within the troposphere, is constant within the tropopause, and then increases with altitude within the stratosphere. Woods (1988) accounted for this structure, and removed some simplifications that had been made in earlier theories (Wilson et al., 1978; Settle, 1978; Sparks, 1986). Within the framework of steady, one-dimensional, single phase flow, the column height can be directly related to the mass flux of material out of the vent. Figure 13 illustrates this relationship for two eruption temperatures (800 and 1200 C; note that the dashed curves are from the work of Settle, 1978, while Woods' results are solid curves, and the dots are data from actual eruptions). These calculations assume eruption into a dry atmosphere, the importance of which will be explained in the next section. Column height increases with increasing mass flux and eruption temperature because these are the main determinants of the buoyancy that is available to drive the column upward above the gas thrust region. Often when an eruption occurs we have some data on column height from satellite and other observations. Figure 13 can provide a quick means of estimating mass flux from these data.

6.5 Influence of atmospheric moisture on buoyant eruption columns

We have seen that entrainment of air is of fundamental importance in driving buoyant eruption columns upward until they reach a level of neutral buoyancy. The theoretical results reviewed thus far have been based on one-dimensional, steady flow of a pseudogas into a dry atmosphere, so that dry air is entrained. In nature, though, many (if not most) eruption columns penetrate atmosphere containing some water vapor. This is especially true in humid coastal and tropical to subtropical environments. Thus water vapor is entrained into the columns with the air. As this entrained water vapor continues to rise, and therefore cool and decompress, condensation may occur. Condensation releases latent heat that can add buoyancy to the eruption column and drive it to higher altitudes than if the atmosphere were dry.

Two recent models (Woods, 1993a; Glaze et al., in press) have considered the effects of condensation (moist convection) on eruption column dynamics. The models are somewhat different in their assumptions, but the significant results are similar. The Glaze et al. (in press) model allows the pseudogas to consist of four components -- dry air, water vapor, liquid water drops, and solid particles -- each of which is tracked by a mass conservation equation as is the bulk mixture. Conservation of momentum and energy are maintained for the mixture. They allow the condensation rate to vary between zero and a maximum that implies that condensation takes place instantaneously so that the vapor phase is maintained just at saturation. The model of Woods (1993a) assumes the latter end member, arguing that abundant ash particles provide ample nucleation sites for condensation.

Figure 14 illustrates one of the important effects of moist convection on eruption columns. These calculations, from Woods (1993a), are for eruptions with the same vent exit velocity of 50 m/s, but varying mass flux rates (ranging from ~10^3 to 10^8 kg/s) and three different atmospheric water vapor contents (20%, 50%, and 100% relative humidity). From Figure 14a it is apparent that eruptions with mass discharge rates less than about 10^7 kg/s (Hawaiian, Strombolian, and weak Vulcanian eruptions) are quite sensitive to atmospheric humidity. For example an eruption rate of 10^4 kg/s will rise to an altitude of about 2 km if the atmosphere is relatively dry (20% relative humidity), but will rise to 5 km if the atmosphere is saturated with water vapor, due to the release of latent heat as the entrained water condenses. Another illustration of these effects is shown in Figure 14b, where it can be seen that for the case where an eruption column rises to 5 km through a saturated atmosphere, the mass of entrained water vapor at the top of the column can be 2-10 times that of the original erupted mass. On the other hand, for an eruption column rising to about 2 km altitude through an atmosphere of 20% relative humidity, the mass of entrained water at the top is only a fraction of the original erupted mass. Eruptions with mass discharges exceeding about 10^7 kg/s are insensitive to the atmospheric water vapor content because the total mass of vapor that can be entrained is a small fraction of the total erupted mass.

Glaze et al. (in press) presented results for two different eruption discharge rates into atmospheres with two different water vapor contents (defined as "wet" and "dry"), and compared results for no condensation, moderate condensation rate, and rapid condensation. As was also shown by Woods, they

demonstrate that eruptions with rates larger than about 10^7 kg/s are only minimally affected by condensation, although they are affected by the atmospheric moisture loading because this affects the temperature profile in the atmosphere. Table 2 describes the affects of atmospheric moisture loading and condensation rate on an eruption of 1.7×10^7 kg/s. In this case column height is most sensitive to the atmospheric moisture because of its effects on temperature profiles. The atmospheric moisture also strongly determines the fraction of original erupted water vapor at the column top versus that which is entrained; for a dry atmosphere the water at the top is 74% erupted, while for a wet atmosphere only 30% of the water at the column top was erupted from the vent -- the remaining water was entrained. For cases where condensation is rapid, 81-90% of the water at the column top is condensed. Another important result of Glaze et al.'s calculations is the quantity of water vapor that is redistributed from lower altitudes to the altitude of the column top. They showed that for eruptions that penetrate into the stratosphere, the water vapor brought into the stratosphere by a single eruption rivals all other common sources of water in that part of the atmosphere.

7. Time-dependent dynamics with constant eruption rate

As I have stated many times, the theory described in Section 6 above involves several simplifications of eruption column physics, the most important of which are steady, one-dimensional flow, and the treatment of the multiphase mixture as a single fluid (pseudogas). There has been a growing field of research in theoretical volcanology in the past decade that seeks to relax these simplifications. In essence, this work is approaching the level of complexity that is presented in the governing equations of Section 3. The main thrust of this work, which I review below, is to account for at least two phases (gas and particles of one size), two dimensions, and to allow time-dependent behavior. We begin by exploring time-dependent eruption column behavior when the discharge conditions at the vent are held steady, briefly followed by phenomena when the discharge itself is time-dependent as well.

7.1 Fountain evolution and pyroclastic flow inception

A number of recent studies have used numerical techniques to study the evolution of eruption columns that collapse (Valentine and Wohletz, 1989; Valentine et al., 1991, 1992; Dobran et al., 1993; Neri and Dobran, 1994). With regard to the governing equation set presented here, these studies have allowed time dependence, are two-dimensional (cylindrical symetry), and include two-phase flow of water vapor and particles of a single size. The particles and gas each have a set of mass, momentum, and energy conservation equations; slip velocities and heat transfer between the phases is allowed although to date mass transfer has not been modeled in this approach. The work of Valentine and Wohletz (1989) and Valentine et al. (1991, 1992) made a further simplification where the erupting gas and atmosphere were treated as the same ideal gas. The Dobran et al. (1993) and Neri and Dobran (1994) model is similar in its basic approach to the Valentine and Wohletz (1989) and Valentine et al. (1991, 1992) model, but with some important refinements. From the perspective eruption columns, the most important of these refinements is the treatment of the vapor phase as consisting of two components, H_2O vapor erupted from the volcano, and air. This allows more rigorous treatment of buoyancy effects in the eruptions.

Figure 15 illustrates the "near-field" evolution of a collapsing eruption column, or fountain, reported by Valentine and Wohletz (1989). For this calculation the following conditions where used: vent exit velocity, 300 m/s; particle volume fraction at vent, 0.01; vent pressure equal to atmospheric; vent radius, 200 m; particle radius, 0.01 cm; eruption temperature, 1200 K; constitutive equations and material properties can be found in Valentine and Wohletz (1989). Figure 15 shows contours of four variables (particle concentration, gas pressure, gas density, and particle temperature) at three different times after the beginning of the eruption. Note that the calculations assume cylindrical symmetry, such as could occur in a central-vent eruption, so that the plots are cross sections through one side of the numerical eruption and the left-hand axis of the plots is the symmetry axis. When any jet or plume penetrates an ambient fluid, in this case the atmosphere, a rolling vortex forms at the head as the flow pushes the ambient out of its way. Valentine and Wohletz used the term "working surface" to discribe this region of the flow field.

Ten seconds after the numerical eruption begins, the working surface has risen to between 2 and 3.5 km altitude, forming a rolling vortex. The edge of the column is diffused due to turbulence and

numerical diffusion. Velocity vectors (tick marks in the figure, oriented parallel to flow direction and length proportional to speed) show a rapid deceleration toward the top of the column along the vertical axis. This deceleration produces high pressure regions in the flow as kinetic energy is converted to a stagnation pressure. The pressure contours also show a hemispherical blast wave propagating into the atmosphere, triggered by the initial impulse of the column as it penetrates the atmosphere. This wave propagates out of the model domain a few seconds later.

At a time of 80 s into the eruption, the column has spread laterally at an elevation of 3.5-4 km, where its initial kinetic energy has been spent. Because the gas-particle mixture is still denser than the atmosphere at this altitude, the laterally-spreading part begins to collapse back to the ground. At the elevation of collapse, vertical velocity along the symmetry axis has decreased to zero, resulting in a high (stagnation) pressure region. A vortex develops at the head of the collapsing flow (this region, where the eruptive mixture flows downward, is referred to as the "stem"); when the stem impinges on the ground this vortex will become the head of the resulting pyroclastic flow. Significant quantities of ash continue to rise above the developing fountain as a buoyant co-ignimbrite plume. This plume is a result of turbulent mixing (entrainment) and heating of ambient on the margins of the fountain, which rises and drags with it some ash.

By 140 seconds, a distinctive fountain geometry has developed, feeding pyroclastic flows that move laterally across the ground. A high (stagnation) pressure region is present where the stem of the fountain impinges on the ground; this high pressure provides a force to propel the pyroclastic flow laterally, in addition to the flow's higher-than-atmospheric density. Note that the stem impacts the ground some distance from the vent and that pyroclastic flows move both radially outward and inward from that point. Valentine et al. (1992) analyzed ~30 numerical fountain-forming eruptions and found that this initial impact distance (defined as the point where ash velocity is zero and ground flows move away from in both directions) is typically equal to the initial fountain height minus a few hundred meters (Figure 16). In detail the dynamics of compressible, two-phase fountains involve a complex interplay between exit pressure and particle settling velocity as well as exit velocity, vent radius, and gas content. The scatter in Figure 16 is due variations in these factors,which influence both fountain height and impact distance. For

example, holding all other factors constant, the ratio of impact distance to fountain height will be reduced by an increase in particle size. The gas density plot in Figure 15 shows that the fountain results in hot, less dense gas being dragged by the particles beneath relatively cooler, denser atmosphere. The ramifications of this for column dynamics are discussed below. The dynamics of pyroclastic flows are discussed in the paper by Freundt and Bursik in this volume.

7.2 Unsteadiness in fountain height

Figure 15 shows that pyroclastic flows originating from column collapse (fountaining) consist of two main components, one of that flows radially outward and another that flows back toward the vent to be recirculated into, and thereby affecting, the eruption column and in turn feeding back into the fountain dynamics. Figure 17 illustrates these effects in terms of fountain height (defined as the altitude where vertical particle velocity equals zero along the symmetry axis) for a simulated eruption with the following conditions (Valentine et al., 1992): exit velocity, 290 m/s; gas (H_2O) mass fraction, 1.7%; exit pressure equal to atmospheric; vent radius, 200m; particle radius, 0.01 cm, exit temperature, 1200 K. The gas thrust part of the column initially reached an altitude of about 4 km, and began collapsing from an altitude of about 3.5 km. With only a minor fluctuation, the fountain height, shown as the solid line in Figure 17, remains relatively constant at about 3.5 km for about 170 s into the eruption. During this time the stem is forming and falling, eventually impacting the ground at a time of about 140 s at a distance of about 3.2 km from the vent, shown by the beginning of the dashed line in Figure 17. At this time pyroclastic flows begin to move outward and inward. The inward-flowing component travels at about 100 m/s toward the vent, reaching it at a time of about 170 s into the eruption. This material is reincorporated into the base of the eruption column, where it is accelerated upward. This acceleration extracts some of the upward momentum from the column, resulting in a gradual decrease in fountain height with time; because of this, the impact distance also decreases with time (Figure 17). The somewhat step-like decrease in fountain height represents "waves" recirculation as the stem of the fountain underwent changes in its shape.

Dobran et al. (1993) and Neri and Dobran (1994) conducted a detailed analysis of the evolution of fountain height with time. Figure 18 shows results for one of the numerical eruptions reported in Dobran

et al. (1993). They used both gas pressure and mixture density to define the fountain top. Figure 18a shows time evolution of the fountain top defined by pressure (both where the flow pressure equals atmospheric pressure, and at the location of maximum pressure due to stagnation), whereas Figure 18b uses mixture density (maximum density and location where density equals atmospheric). In both plots we see that the fountain initially rises to its maximum altitude, and then oscillates with a period of about 40 s as it gradually declines. Figure 18c diagrammaticaly shows how material is recirculated. For material to go through single cycle of exiting the vent, rising to the fountain top, falling through the stem, and flowing back to the column base it must travel a distance of approximately four fountain heights. The time to travel this distance defines the oscillation period, t_{cycle}, and can be estimated by

$$t_{cycle} \approx 2v_{exit}/g \quad , \tag{26}$$

where v_{exit} is the velocity of the eruptive mixture as it exits the vent, and g is gravitational acceleration. In a sense, each oscillation in Figure 18 is a recirculation of the first cycle. For the eruption upon which Figure 17 is based, from Valentine et al. (1992), equation 26 would yield an estimate of $t_{cycle} \approx 60$ s. This corresponds well with the period of the step-like changes in fountain height in Figure 17. It is important to note that some combinations of eruption parameters produce only one or two oscillations after the initial drop in fountain height (e.g., eruption A in Dobran et al., 1993), while others exhibit a more step like decline (as in Figure 17) that may ultimately reach a steady height, and others, like that shown in Figure 18, may develop a continuously oscillating fountain. A crucial point, though, is that even though the simulated eruptions are held at constant vent conditions, the resulting pyroclastic flows may exhibit complex pulsing behavior. Detailed analysis of the effects on pyroclastic flows has been presented by Neri and Dobran (1994), but review of this is beyond the scope of this paper.

7.3 Unsteadiness in coignimbrite plumes

Figure 15 shows how a collapsing eruption column, where the majority of the eruptive mixture forms a fountain and laterally-moving pyroclastic flows, can still produce a buoyant plume (called a "coignimbrite" plume because it is part of the eruptive process that produces ignimbrites) due to entrainment and heating of air along the margins of the fountain. This air, along with some of the erupted gas, rises buoyantly and drags some particles upward with it. This coignimbrite plume has as its source the entire fountain and the surface of the pyroclastic flows. For steady-discharge eruptions there are at least four sources of unsteady behavior in the coigmibrite plume: (1) variations due to recirculation within the fountain, (2) ash that is swept inward off the top of pyroclastic flows by eruption-induced winds, (3) internal waves reflected inward when pyroclastic flows incounter topographic obstacles, and (4) water vapor buoyancy effects over pyroclastic flows (phoenix plumes).

Valentine et al. (1991) considered the first three sources of unsteadiness listed above. Figure 19 shows the time variations in mass flux of ash (kg/s) rising through two elevations in a simulated collapsing column (the mass flux is normalized to that being discharged from the vent). The top plot, 4 km altitude, is at the initial height of column collapse at early times but after about 70 s the fountain is below this altitude and the mass flux is that of the buoyant coignimbrite plume. The lower plot records mass flux in the gas thrust part of the fountain. The eruption conditions at the vent are: exit velocity, 300 m/s; H_2O mass fraction, 0.74%; exit pressure equal to atmospheric; temperature, 1200 K; particle radius, 1 cm; vent radius, 200 m. In one calculation, the terrain surrounding the vent is flat, while in the second calculation there is a 500 m high barrier at a distance of 4 km from the vent. Further details can be found in Valentine et al. (1991).

The mass flux in the coignimbrite plume at 4 km has its highest value (~50% that at the vent) when the working surface first passes through that altitude; it then falls rapidly off to values of several percent, showing how the coignimbrite plume transports a small portion of the total erupted material (although this is exaggerated in our calculation because of the relatively large particle size which is not easily lofted). About 180 s into the eruption, the mass flux at 4 km begins to increase. For the calculation with flat terrain (dashed line in Figure 19) the flux increases to a peak of ~7% of the vent flux at 260 s. It then

decays gradually back, with a slight tertiary increase at ~310 s, to an apparently steady value of ~2%. This secondary peak is attributed partly to propagation of the mass flux peak recorded ~60 s earlier at 0.4 km, in the gas thrust part of the fountain. This peak at 0.4 km is caused by reincorporation of the first pulse of ash that collapsed through the fountain and flowed back to the vent. Another significant component of the secondary and tertiary peaks at 4 km is likely due to ash that is entrained by eruption induced winds which flow radially inward to feed the hot coignimbrite plume. This is supported by the fact that the peak decays smoothly after 310 s even though the inner fountain continues to oscillate at 0.4 km.

For low-level (0.4 km) mass flux unsteadiness the effect of the topographic obstacle is very small during the simulated eruption time (compare solid and dashed lines in Figure 19). This reflects the fact that the fountain and its recirculation zone are well within the obstacle, which, therefore, mainly affects the outward-moving pyroclastic flows. However, the coignimbrite plume, at 4 km, experiences its secondary peak about 40 s earlier than the flat terrain case, and it is a stronger peak reaching about 10% of the vent mass flux. This difference is attributed to the gravity wave that is reflected ventward when the pyroclastic flow encounters the topographic obstacle. This wave propagates along the top of the pyroclastic flow and enhances ash entrainment up into the coignimbrite plume.

It is important to consider these sources when interpreting the dynamics of remotely observed plumes and their deposits. Remote observations of eruptions commonly record parameters related to cloud temperature (e.g. infrared intensity), ash concentration (opacity), and size. Figure 20 shows temporal evolution of temperature and ash concentration on the plume axis, as well as the coignimbrite plume radius, at an altitude of 7 km (top of the computational domain) for the two calculations described above. The plots of gas and ash temperature are qualitatively similar; the first peak in gas temperature occurs at about 100 s when the main part of the plume head passes through that elevation. Note the large degree of thermal disequilibrium between particles (ash) and gas at early times, a result of the large particle size and therefore relatively inefficient interphase heat transfer. At later times the gas and ash temperatures follow more similar trends (although still with different temperatures). This is because at later times the fountain structure is established, and most gas and particles that rise to 7 km have traveled through the fountain and outward in pyroclastic flow before being swept up into the coignimbrite plume, thus having more time to

approach equilibrium. Differences between the flat terrain and obstacle cases do not show up at 7 km altitude until about 180 s into the eruption. After this the temperatures for the two cases are somewhat different. A secondary peak in temperature occurs at about 260 s for the flat terrain case, about 40 seconds later than the obstacle case and with temperatures that are higher by about 30 and 60 K for gas and ash, respectively. This again reflects the different sources of unsteadiness that dominate the two cases. In the flat terrain case the secondary pulse into the coignimbrite plume is partly fed by the material that has been recirculated in the fountain below. This material was relatively unexposed to cool atmosphere and therefore hotter when it was fed into the coignimbrite plume. In the obstacle case, though, the secondary pulse is strongly influenced by the reflected gravity wave which draws material from the top of the pyroclastic flows, where it has been exposed to the cool atmosphere, into the coignimbrite plume.

Ash concentration and coignimbrite plume radius (Figure 20c,d) show that the secondary pulse for both cases has similar ash loadings, but that the secondary "bulge" of in plume size is larger for the obstacle case (this accounts for the larger mass flux peak that is also seen in Figure 19) due to the reflected gravity wave. Interestingly, after the secondary radius pulse has passed the no-obstacle case "relaxes" to a larger radius (2.4 km vs. 1.7 km) than the obstacle case. This results from the larger areal extent of the pyroclastic flows that feed the coignimbrite plume when they are not impeded by topography. When observing these variations remotely, one might infer multiple pulses or eruptions at the vent, when in reality the eruptive discharge itself is constant.

As mentioned earlier, Dobran and colleagues have developed a refined two-phase flow model that, among other improvements, accounts for two components in the vapor phase - water vapor (erupted from the vent) and air. This allows more accurate modeling of buoyancy effects in eruption columns. One of the ways that this is manifested is in the development of "phoenix plumes." Figure 21 shows the evolution of an eruption at several times, using contours of the logarithm of ash volume fraction. The vent conditions for this simulated eruption are: vent radius, 300 m; temperature, 1200 K; exit velocity, 200 m/s; exit pressure equal to atmospheric; particle volume fraction, 0.01; particle diameter, 0.001 cm; further details of the model can be found in Dobran et al. (1993; their eruption B). During the first 60 s of eruption (Figure 21), a fountain develops, collapsing from a height of about 2 km. At later times,

pyroclastic flows move radially away from the vent. As particles settle downward in the flows, hot, relatively clean water vapor forms plumes over the pyroclastic flows. These pheonix plumes (so called because they rise from the ash) rise, dragging a small quantity of ash with them, and are slowly drawn inward to join the central coignimbrite plume. Figure 22 illustrates the same process in the same simulated eruption, but showing contours of water vapor concentration (note different scales than Figure 21). Each pheonix plume produces a pulse in the coignimbrite plume, and they also influence the lateral movement of the pyroclastic flows. As the pyroclastic flows move farther away from the vent, phoenix plumes tend to rise straight up from the flow so that a remote observer would see a continually widening eruption cloud.

7.4 Transition from collapsing to buoyant columns

In Section 6.2 we reviewed the criteria for buoyant versus collapsing columns within the context of steady state, one-dimensional models. Neri and Dobran (1994) have explored the transient behavior of eruptions near the critical conditions that define whether a column collapses or is buoyant, using the Dobran et al. (1993) model. We have already seen examples of simulated eruptions that are well within the range of collapsing or fountaining behavior in Sections 7.1-3. Figure 23 shows, using gas temperature contours, the behavior of an eruption column that is right at the transition from collapsing to buoyant behavior (eruption B5 of Neri and Dobran, 1994). During the first 100 s the column rises to about 5 km where it begins to collapse. However, the stem is just barely denser than air. As it begins to fall, it heats the air around it which rises and mixes with the upper stem to make it buoyant. Thus the initial part of the stem detaches and falls to the ground (forming a small scale density current there), while the trailing parts of the stem become first neutrally buoyant (spreading horizontally) and then positively buoyant so that it rises and drifts toward the symmetry axis to join the central plume. Subsequent material fed into the stem is at first negatively buoyant, and the cycle is repeated - partial collapse followed by buoyant rise.

Figure 24 shows particle concentration and gas temperature at three different times for a column that just meets the criteria for buoyant rise. We see that initially, up to times of about 100 s, the column behaves as the one describe above; the mixture is barely denser than air at at the top of the gas thrust region

(~2.1 km altitude). A "blob" of mixture begins to fall to the ground, but it entrains and heats sufficient air to make itself, as well as trailing material in the stem, buoyant. Figure 25 shows evolution (gas temperature contours) of an eruption that is farther into the realm of buoyant behavior. Only a small part of the column is temporarily slightly denser than air at the top of the gas thrust region (~5 km), and a buoyant column develops quite easily. Figure 26 compares the column collapse criteria for different eruptive water vapor contents determined from the numerical studies of Neri and Dobran (1994) with those of previous workers. The Neri and Dobran results suggest that columns exhibit less buoyant behavior than predicted by the Woods (1988) model described in Section 6. It is likely that this difference reflects the assumptions of perfect momentum and heat coupling between gas and particles (pseudogas) in the Woods model.

7.5 Time-dependent, three field (two particle sizes)

Neri and Macedonio (1996) recently made a major advance in numerical modeling of eruption columns by adding a second particle field to the model of Dobran et al. (1993). The new model is thus a three-field model with a set of conservation equations for the vapor phase, and for each of two particle populations. They retain the two-component (water vapor and air) model for the vapor phase. In addition they accounted for the drag that one particle field exerts on the other with a constitutive equation based on conservation of linear momentum between colliding particles (Equation 25 of Neri and Macedonio, 1996).

To elucidate the effects of accounting for two particle sizes, Neri and Macedonio carried out three eruption simulations where all vent and boundary conditions were identical, and only particle size was varied. Vent conditions for the three eruptions were as follows: vent radius, 50 m; eruption temperature, 1200 K; exit velocity, 120 m/s; pressure equal to atmospheric; H_2O mass fraction, 0.8%; total volume fraction of particles, 0.01. In their eruption A1, the particle diameter was set at 10 μm, a small size that is closely coupled to the gas phase. Figure 27 illustrates this simulated eruption with contours of the logarithm of particle concentration. The gas thrust portion of the column initially rises to about 0.7 km altitude, where its initial kinetic energy is spent and it begins to collapse. The stem falls to the ground and feeds pyroclastic flows. A large phoenix plume of hot water vapor forms over the top of the flow at a

distance of about 3 km from the vent; because of the small particle size the plume is able to drag up with it a relatively large quantity of ash. As the plume is drawn back toward the central coignimbrite plume the combination of accompanying inward wind and depletion of ash from the pyroclastic flow by the phoenix plume causes the pyroclastic flow to stop at a distance of about 5 km from the vent. For the remaining duration of the numerical eruption ash rises in a large coignimbrite plume.

Figure 28 shows simulated eruption A2 with the same conditions except the particle size is 200 μm, again focusing on particle concentration. At early times the eruptions are quite similar, however at later times particles are much more concentrated in a denser pyroclastic flow in A2 than in A1. Plots of water vapor concentration (not shown here) show that phoenix plumes develop in a similar way to eruption A1, but they are basically ash-free. This all reflects the coarser particle size that is less well coupled to the gas phase. The resulting coignimbrite plume (at least the ash-laden part that would be visible in a real eruption) in A2 is much narrower than in A1. Also the A2 pyroclastic flows are relatively unaffected by phoenix plumes.

Figures 29 and 30 show evolution of the same eruption conditions but with a combination of the two particle sizes, 0.005 volume fraction for 10 μm, and 0.005 volume fraction for 200 μm particles (eruption A3). Figure 29, concentration of the small particles, illustrates the effect of drag of the larger particles on the smaller ones. The small particles are dragged along in the pyroclastic flow for a distance of 6.5 km during the duration of the eruption (compared with stopping at 5 km in Figure 27). At the same time, the small particles are drawn up into a large phoenix plume as in A1. The larger particles are also affected by the smaller ones, as can be seen by their reduced travel distance in the pyroclastic flow in A3 (Figure 30) compared to A2. Also, some of the coarser particles (albeit at a low concentration) are drawn up into the phoenix plume in A3, unlike in eruption A2, to contribute to the large central coignimbrite plume. A major area for future work in eruption column and pyroclastic flow modeling is to continue adding particle populations so that these coupled behaviors can be more realistically modeled.

8. Time-dependent dynamics with transient eruption rate

The effects of various parameters (vent radius, temperature, gas content, velocity) as an eruptive mixture exits the vent have been described above both within the context of assumed steady flow (Section 6) and within the context of steady discharge but time-dependent column dynamics (Section 7). The effects of temporal variation in these parameters can be discussed within the first context as long as it is assumed that the variations occur very slowly, at a rate such that the response to any increment of change can be propagated the entire height of the eruption column before the next increment of change occurs. Relatively little work has been done on the effects of transient vent conditions that occur on more rapid time scales; here I provide a brief review of this work.

8.1 Unsteady conditions at the vent

Anilkumar et al. (1993) reported a set of experiments that raises the question, does steady flow ever occur in natural eruptions? Their experiments studied the dynamics of a mixture of solid particles and gas as the mixture is accelerated upward by gas expansion, much as would occur in a volcanic conduit. They found that even though the particles are evenly distributed macroscopically prior to accleration, they rapidly become heterogeneously dispersed as the mixture accelerates upward. During the initial stages of acceleration, the particles accelerate upward as discrete sheets or layers (Figure 31). As they continue to acclerate upward and interact with the expanding gas the layers are stretched vertically and distorted to form sheet and ribbon-like regions of high particle concentration separated by regions of relatively clean gas (Figure 32). High in the shock tube in which the experiments were conducted pressure and particle concentration fluctuated widely with time, recording passage of the mixture heterogeneities. If we accept that these experiments provide a partial analog for the acceleration of ash up a volcanic conduit, then we can expect that the conditions at the vent will be highly transitory, with ash-rich "slugs" being discharged and separated by slugs of relatively clean gas. If these phenomena have a relatively high frequency, say higher than the frequency of the dominant eddies in the eurption column, the transitory discharge may be rapidly mixed and homogenized in the base of the eruption column. On the other hand, if the discharge fluctuations have relatively longer time scales they may not be homogenized in the eruption column and

will produce major fluctuations in the column dynamics. Many implications of this are discussed by Anilkumar et al. (1993).

8.2 Influence on eruption columns

In Section 6.3 I reviewed some of the experiments of Kieffer and Sturtevant (1984) on the gas thrust part of eruption columns, but focusing on the establishment of steady state, compressible flow features (e.g., Mach disk shocks). Kieffer and Sturtevant also discuss the transient behavior of the jets between the time of flow initiation and establishment of steady state, and the reader is referred to their paper for further information on this. One important feature that they discuss is eruptions of very short duration in which most of the ejected ash rises in the working surface, or start-up vortex, structure. This is very common in Vulcanian and Strombolian bursts.

Valentine and Wohletz presented an example compuational eruption that formed a fountain and pyroclastic flow (Figure 33). Fifty seconds into the eruption the column is beginning to collapse at an altitude of about 2 km, and the eruption discharge is turned off. At 70 s most of the erupted material (contained within the innermost contour of particle volume fraction) is falling back to the ground and moving outward as the beginning stages of a pyroclastic flow. At 100 s the pyroclastic flow is continuing to move outward but tapers off toward the vent. A coignimbrite plume continues to rise above the vent as long as the pyroclastic flow is active, demonstrating that the end of eruptive discharge would be difficult to determine from remote observations.

9. Influence of the ambient medium

Thus far I have only reviewed the dynamics of eruption columns that are injected into simple atmospheres with no wind, with the exception of Section 6.5 which discused influence of atmospheric moisture on columns. Even within this simple treatment of the atmosphere eruption column physics are quite complex and much remains to be learned. However, it is clear that in Nature the atmosphere rarely follows this idealized treatment. The structure of the atmosphere varies with latitude and season, and this in turn affects the efficiency of entrainment and rise heights. Quite commonly eruption columns penetrate

an atmosphere with a cross wind, and the direction of this wind can vary with altitude, distorting an eruption column in complex ways. An added complication is that many explosive eruption columns must penetrate a body of water before entering the atmosphere; such is the case for eruptions through caldera lakes or shallow seas. The effects of these different ambient conditions are just beginning to be studied, and are briefly reviewed below.

9.1 Effects of latitude and season

Eruption columns that are not strong enough to penetrate the tropopause are most sensitive to latitude and season. Glaze et al. (in press) present results for the steady state column height of eruptions at several latitudes and seasons, shown in Table 3. The calculated column heights in Table 3 are for an eruption with the following vent conditions: temperature, 1000 K; exit velocity, 300 m/s, vent radius, 20 m; exit pressure equal to atmospheric; the model used is a single phase (pseudogas), steady state model. The table shows the tropopause altitude, neutral buoyancy height (NBH, where the density of the column equals that of the local atmosphere), and the maximum rise height (H, somewhat higher than NBH due to momentum of the column). A major source of the difference in NBH and H between lattitudes and seasons is the temperature of the atmosphere. A column rising into a warm (e.g., summer or low latitude) atmosphere will have a smaller temperature difference and therefore smaller buoyancy force relative to an eruption into a cold atmosphere.

9.2 Cross wind

As mentioned in the Introduction a buoyant column eventually reaches an altitude where its density equals that of the air, and at this level the column spreads laterally as a suspended density current called an umbrella cloud (similar to an anvil cloud at the top of a thunderstorm cell). In a calm atmosphere the column axis will be vertical and the umbrella will be circular in plan view and centered directly over the vent. A cross wind will displace a column in the downwind direction, as illustrated in Figure 34; Carey and Sparks (1986) analyzed this process and its effects on fallout distribtion (discussion of the latter is deferred to the paper by Rosi in this volume). The column axis is deflected from the vertical by a distance

d, measured at the base of the umbrella region. Material flowing laterally in the umbrella will flow upwind until its speed equals the wind speed; this is referred to as the stagnation point. On the downwind side of the column the umbrella will continue to spread, assisted by the wind. In plan view, then the umbrella would have an elliptical shape.

If the lateral velocity of material flowing into the umbrella is less than the wind speed to begin with, the entire umbrella region will be deflected downwind, forming a "bent-over" plume. If material flows laterally into the umbrella at exactly the wind speed then the column forms a "straight-edge" column. Figure 35, from Carey and Sparks (1986), illustrates the three types of behaviors in terms of the ratio of the distance between column axis and stagnation point to *d*, and the height of the base of the umbrella. The curves are for three different wind speeds.

An interesting topic that, to my knowledge, has not been investigated is the coupling between the cross wind and plume height. For example, the analysis of Carey and Sparks (1986), which is an imporatnt first step, used column properties based on a steady-state, one-dimensional model with a calm atmosphere, and simply displaced the columns downwind according to the wind velocity. This assumes a linear coupling, and that the cross wind has no effect on processes such as entrainment and particle distribution. However, one can imagine more complicate effects, such as the wind stripping off the dilute and cool margins of the column and more directly accessing the hotter interior on the upwind side and perhaps enhancing mixing there and thus affecting column height. Such complications are indicated by the work of Ernst et al. (1994), who explored the phenomenon of plume splitting. This occurs when a cross wind causes to counter-rotating vortices, one on each side of an eruption column, that drift apart as the column is transported downwind so that when viewed from above the column splits into two parts.

9.3 Eruption through water

Eruption through a body of surface water is just beginning to be studied in detail. Koyaguchi and Woods (1996) studied the effects of incorporation of different mass fractions of surface water into eruption columns. The quantitative results of their study are beyond the scope of this paper, but their qualitative results are illustrated in Figure 36. A small mass fraction of water added to an eruption column

will completely vaporize and therefore promote buoyant behavior, whereas larger quantites of water only incompletely vaporize and cool the eruption column so that it will tend toward collapsing behavior. There is a regime of magma mass flux where a "dry" eruption will collapse, but a slight addition of surface water will drive it to high-standing buoyant behavior. The Koyaguchi and Woods (1996) paper is a critical first step in addressing this problem. A next step will involve exploring the fluid dynamics of mixing of surface water into an eruptive jet, a process which must be sensitive to the same parameters as are important to entraiment of air (vent radius, velocity, particle loading at the vent). This will elucidate the range of mass fractions of entrained water that are possible for a given eruption.

10. Conclusion

In this paper I have attempted to review the major points of our understanding of eruption column dynamics. I have focussed on the most recent work, all of which builds upon many works that I have not explicitly referred to. To return to the theme of multifield flow and the governing equations laid out in Section 3, I believe it is most fruitful to use such a set of equations as a way of integrating the different approaches taken by researchers and as a "measuring stick" for the assumptions and simplifications of each approach. Certainly one of the most promising avenues of research is to continue toward numerical solution of the full set of equations in a step-by-step manner. We are reaching a point where future steps will require extensive research to expand our base of constitutive equations such as particle-particle interaction, multifield turbulent transport and mass transfer rates. Similarly, numerical techniques will likely need to be updated in order to tackle the equations as laid out in this paper; the advent of teraflop (10^{12} floating point operations per second) computing systems this year will provide ample hardware. Such research will serve as an important link to the general continuum mechanics and applied mathematics communities.

References

Anilkumar AV, Sparks RSJ, Sturtevant B (1993) Geological implications and applications of high-velocity two-phase flow experiments. *Journal of Volcanology and Geothermal Research*, 56: 145-160.

Bird RB, Stewart WE, Lightfoot EN (1960) *Transport phenomena.* John Wiley and Sons, New York, 780 pp.

Brown GL, Roshko A (1975) On density effects and large structure in turbulent mixing layers. *Journal of Fluid Mechanics*, 64: 775-816.

Carey SN, Sparks RSJ (1986) Quantitative models of the fallout and dispersal of tephra from volcanic eruption columns. *Bulletin of Volcanology*, 48: 109-125.

Dobran F (1992) Nonequilibrium flow in volcanic conduits and applications to the eruptions of Mt. St. Helens on May 18, 1980, and Vesuvius in A.D. 79. *Journal of Volcanology and Geothermal Research*, 49: 285-311.

Dobran F, Neri A, Macedonio G (1993) Numerical simulation of collapsing volcanic columns. *Journal of Geophysical Research*, 98: 4231-4259.

Ernst GGJ, Davis JP, Sparks RSJ (1994) Bifurcation of volcanic plumes in a cross wind. *Bulletin of Volcanology*, 56: 159-169.

Foshag WF, González-Reyna JR (1956) Birth and development of Parícutin volcano, México. *U.S. Geological Survey Bulletin*, 965D: 355-489.

Francis P (1993) *Volcanoes: a planetary perspective.* Clarendon Press, Oxford, 443 pp.

Glaze LS, Baloga SM (1996) Sensitivity of buoyant plume heights to ambient atmospheric conditions: implications for volcanic eruption columns. *Journal of Geophysical Research*, 101: 1529-1540.

Glaze LS, Baloga SM, Wilson L (in press) The transport of atmospheric water vapor by volcanic eruption columns. *Journal of Geophysical Research.*

Kieffer SW (1981) Fluid dynamics of the May 18 blast at Mount St. Helens. In *The May 18, 1980 Eruption of Mount St. Helens* (Lipman PW, Mullineaux DR, eds.), U.S. Geological Survey Professional Paper 1250: 379-400.

Kieffer SW, Sturtevant B (1984) Laboratory studies of volcanic jets. *Journal of Geophysical Research*, 89: 8253-8268.

Koyaguchi T, Woods AW (1996) On the formation of eruption columns following explosive mixing of magma and surface water. *Journal of Geophysical Research*, 101: 5561-5574.

Li W-H, Lam S-H (1964) *Principles of fluid mechanics*. Addison-Wesley Publishing Co., Inc., London, 374 pp.

Luhr JF, Simkin T (1993) *Parícutin: the volcano born in a Mexican cornfield.* Geoscience Press, Phoenix, 427 pp.

Macedonio G, Dobran F, Neri A (1994) Erosion processes in volcanic conduits and application to the A.D. 79 eruption of Vesuvius. *Earth and Planetary Science Letters*, 121: 137-152.

Middleton GV, Wilcock PR (1994) *Mechanics in the earth and environmental sciences*. Cambridge University Press, Cambridge, 459 pp.

Neri A, Dobran F (1994) Influence of eruption parameters on the thermofluid dynamics of collapsing volcanic columns. *Journal of Geophysical Research*, 99: 11833-11857.

Neri A, Macedonio G (1996) Numerical simulation of collapsing volcanic columns with particles of two sizes. *Journal of Geophysical Research*, 101: 8153-8174.

Riehle JR (1973) Calculated compaction profiles of rhyolitic ash-flow tuffs. *Geological Society of America Bulletin*, 84: 2193-2216.

Settle M (1978) Volcanic eruption clouds and the thermal power output of explosive eruptions. *Journal of Volcanology and Geothermal Research*, 3: 309-324.

Sparks RSJ (1986) The dimensions and dynamics of Plinian eruption columns. *Bulletin of Volcanology*, 48: 3-15.

Takahashi TJ, Griggs JD (1987) Hawaiian volcanic features: a photoglossary. In *Volcanism in Hawaii* (Decker RW, Wright TL, Stauffer PH, eds.), U.S. Geological Survey Professional Paper 1350: 845-902.

Turcotte DL, Schubert G (1984) *Geodynamics: applications of continuum physics to geological problems*. John Wiley and Sons, New York, 450 pp.

Valentine GA (1994) Multifield governing equations for magma dynamics. *Geophysical and Astrophysical Fluid Dynamics*, 78: 193-210.

Valentine GA, Wohletz KH (1989) Numerical models of Plinian eruption columns and pyroclastic flows. *Journal of Geophysical Research*, 94: 1867-1887.

Valentine GA, Wohletz KH, Kieffer SW (1991) Sources of unsteady column dynamics in pyroclastic flow eruptions. *Journal of Geophysical Research*, 96: 21887-21892.

Valentine GA, Wohletz KH, Kieffer SW (1992) Effects of topography on facies and compositional zonation in caldera-related ignimbrites. *Geological Society of America Bulletin*, 104: 154-165.

Wallis GB (1969) *One-dimensional two-phase flow*. McGraw-Hill, New York.

Wilson L, Sparks RSJ, Huang TC, Watkins ND (1978) The control of volcanic column heights by eruption energetics and dynamics. Journal of Geophysical Research, 83: 1829-1836.

Wilson L, Sparks RSJ, Walker GPL (1980) Explosive volcanic eruptions--IV. The control of magma properties and conduit geometry on eruption column behavior. *Geophysical Journal of the Royal Astronomical Society*, 63: 117-148.

Woods AW (1988) The fluid dynamics and thermodynamics of eruption columns. *Bulletin of Volcanology*, 50: 169-193.

Woods AW (1993a) Moist convection and the injection of volcanic ash into the atmosphere. *Journal of Geophysical Research*, 98: 17627-17636.

Woods AW (1993b) The plumes above basaltic fissure eruptions. *Geophysical Research Letters*, 20: 1115-1118.

Woods AW, Bursik MI (1991) Particle fallout, thermal disequilibrium and volcanic plumes. *Bulletin of Volcanology*, 53: 559-570.

Figure captions

Figure 1. Diagram showing the main parts of an eruption column, with a lower gas thrust or jet region, a buoyant or convective region, and an upper umbrella where the cloud spreads laterally. From Sparks (1986).

Figure 2. Basaltic eruption fountain of Puu Halulu, Kilauea Volcano, Hawaii, on 4 April 1983. Photo by J.D. Griggs, published in Takahashi and Griggs (1987). Note that the vast majority of melt erupted falls back in the fountain to coalesce and form lava flows. Clasts on the margins of the fountain may cool sufficiently to add to the pyroclastic cone around the vent, and a small fraction of fine ash is lofted in a buoyant plume of hot vapor above the fountain.

Figure 3. Vigorous, "violent" Strombolian eruption column at Parícutin volcano (Michoacán, México) on 24 March 1943. Eruption column reaches 6 km altitude. From Foshag and González-Reyna (1956) as reproduced in Luhr and Simkin (1993).

Figure 4. Eruption column above a small, discrete Vulcanian explosion at Sakurajima volcano, Japan, in October 1993.

Figure 5. Diagram of principles of conservation equations in fluid mechanics.

Figure 6. Schematic illustration of the concept of the representative elementary volume (REV) for a fluid containing particles (shown here as crystals). Left side shows a fluid with particles that gradually decrease in concentration to the right. Several boxes of different length scales (ℓ_1,ℓ_2,ℓ_3) are shown. Right side shows measured particle volume fraction as a function of measurement length scale, including microscopic variations at small scales and macroscopic variations at scales larger than the REV. From Valentine (1994).

Figure 7. Effect of Mach number on spreading rates and entrainment in mixing layers. Plot shows data from Brown and Roshko (1974). Solid curve illustrates dependence of spreading rate on density ratio between flow and ambient for incompressible flows, while dashed line accounts for Mach number as well. Right side of figure illustrates effects on mixing layer around a jet for the same density ratios but different Mach numbers.

Figure 8. (a) Column heights as a function of vent velocity, and (b) gas-thrust heights as a function of vent velocity, dashed lines being for collapsing conditions and solid lines for buoyant column conditions. Curves in (a) and (b) are for eruptive gas (H_2O) mass fractions of 0.005, 0.01, 0.03, and 0.05, eruptive temperature of 1000 K, and vent radius of 100 m. (c) Column height as a function of vent radius for vent velocity of 100 m/s, eruption temperatures of 1200 and 800 K, and gas mass fractions of 0.01 and 0.05. From Woods (1988).

Figure 9. Criteria for column collapse as a function of the velocity of at the vent and the erupted mass flux for several values of the thermal disequilibrium between clasts and gas (a value of 1 is pure equilibrium and 0 is no particle-gas heat transfer). From Woods and Bursik (1991).

Figure 10. Effective sound speed for mixture of silicate particles and steam as a function of particle loading, for two different temperatures. Eruption columns will typically have $<10^{-2}$ volume fraction of solids. Calculations assume that the particles are perfectly coupled to the gas.

Figure 11. Schematic illustration of the features of an overpressured jet. From Kieffer and Sturtevant (1984).

Figure 12. Schlieren photographs of a small scale jet experiment from Kieffer and Sturtevant (1984). Test fluid is nitrogent erupting from a 13 cm long reservior (below the frame of the photographs) with an initial pressure of 0.725 MPa, and a jet exit (vent) diameter of 1.5 cm. Top photo is at 1 μs and bottom is at 10 μs after flow initiation. Patterns of shocks and rarefactions are seen as the fluid equilibrates to ambient pressure as it travels up the jet.

Figure 13. Comparison of column heights predicted by Settle (1978, dashed lines) and Woods' (1988) models (solid lines) as a function of mass flux at the vent, for eruption temperatures of 800 and 1200 K. From Woods (1988).

Figure 14. Model calculations of Woods (1993) showing the variation with mass eruption rate of (a) the total column height (solid curves) and associated saturation heights (dashed curves), and (b) the mass flux of water supplied to the top of the column as a fraction of the total mass of material erupted from

the vent. All curves are for eruption temperatures of 1000 K and vent velocity of 50 m/s. Numbers on the curves are the relative humidity of the atmosphere at the base of the column. From Woods (1993).

Figure 15. Numerical simulation of a collapsing eruption column from Valentine and Wohletz (1989), showing four parameters at three different times after eruption initiation (10 s, 80 s, 140 s). Calculations assume cylindrical symmetry, so that the vertical axis on the left side of each plot is the symmetry axis. Top row shows contours of the logarithm of particle volume fraction overlaid on velocity (represented by dashes with length proportional to speed and in direction of flow). Second row shows gas pressure contours, third row is gas density, and bottom row is particle temperature.

Figure 16. Initial fountain height versus imact distance from vent for the collapsing stem, based on numerical simulations of Valentine and Wohletz (1989). Note that this plot shows only the values during the initial phase of fountain formation; in any given simulation the fountain height and impact distance continue to evolve throughout the simulation. From Valentine et al. (1992).

Figure 17. Evolution of fountain height and impact distance with time for an eruption simulation from Valentine et al. (1992).

Figure 18. Timewise distributions of fountain heights and maximum pressure and density in the column of simulated eruption B of Dobran et al. (1993). (a) Fountain heights corresponding to the maximum pressure near the fountain top and the pressure corresponding to atmospheric, along the symmetry axis. (b) Similar distributions of mean density and the associated fountain heights. (c) Sketch showing approximate distance traveled by a parcel of gas or a solid particles during a recycling period. From Dobran et al. (1993).

Figure 19. Plots of solids mass flux at 0.4 and 4.0 km altitude as functions of time for simulated collapsing eruption column (see text for details). Values are given in terms of percentage of vent mass flux. From Valentine et al. (1991).

Figure 20. Centerline values of (a) gas temperature, (b) ash temperature, and (c) ash volume fraction at 7 km altitude as functions of time. Also shown is plume radius as a function of time at 7 km altitude (d). From Valentine et al. (1991).

Figure 21. Distribution of particle volume fraction in eruption B of Dobran et al. (1993) at 30, 60, 180, 300, 600, and 1000 s after eruption initiation. Contours are logarithm of particle volume fraction, and range from 10^{-2} in the innermost contour to 10^{-10} in the outermost.

Figure 22. Distribution of water vapor volume fraction in eruption B of Dobran et al. (1993) at 30, 60, 120, 360, 420, and 540 s after eruption initiation. Contours are logarithm of water vapor volume fraction and range from 10^{0} in the innermost contour to 10^{-10} in the outermost.

Figure 23. Distribution of gas temperature (which closely follows particle concentration in the eruption column) at times of 50, 100, 150, 300, 800, and 1600 s after eruption initiation. The contour level represents the difference between the local gas temperature and the undisturbed atmospheric temperature at ground level, and have values ranging from 800 K (innermost contour) to -70 K (outermost). Eruption B5, from Neri and Dobran (1994).

Figure 24. (a) Particle volume fraction and (b) gas temperature at 50, 100, and 200 s after eruption initiation for simulated eruption A6 of Neri and Dobran (1994). Particle volume fraction contours are logarithms and range from 10-1 (innermost) to 10-8 (outermost), while gas temperature is measured as in Figure 23, and the contours range from 800 K (innermost) to -30 K (outermost).

Figure 25. Gas temperature distribution at 100, 200, 250, and 350 s after eruption initiation (Figure 16 of Neri and Dobran, 1994). Temperature is measured as described in caption for Figure 23, contour values range from 800 K (innermost) to -70 K (outermost).

Figure 26. Relationship between vent velocity and mass flow rate at the transition from collapsing to buoyant eruption columns, comparing the the results from numerical modeling of Neri and Dobran (1994; solid lines) with previous steady-state, single-phase, one-dimensional studies by various workers.

Figure 27. Particle volume fraction distribution at times of 30, 120, 420, and 600 s after eruption initiation for eruption A1 of Neri and Macedonio (1996). Contours are logarithm of particle concentration and range from 10^{-1} (innermost) to 10^{-10} (outermost).

Figure 28. Particle volume fraction distribution at times of 30, 120, 420, and 600 s after eruption initiation for eruption A2 of Neri and Macedonio (1996). Contours are logarithm of particle concentration and range from 10^{-1} (innermost) to 10^{-10} (outermost).

Figure 29. Volume fraction of particles with diameter of 10 μm at times of 30, 120, 420, and 600 s after eruption initiation for eruption A3 of Neri and Macedonio (1996). Contours are logarithm of particle concentration and range from 10^{-1} (innermost) to 10^{-10} (outermost).

Figure 30. Volume fraction of particles with diameter of 200 μm at times of 30, 120, 420, and 600 s after eruption initiation for eruption A3 of Neri and Macedonio (1996). Contours are logarithm of particle concentration and range from 10^{-1} (innermost) to 10^{-10} (outermost).

Figure 31. Early stages of lofting of a bed of glass beads initially at rest on a solid plate. First five frames show an experimental run where the top of the bed was initially at the middle of the frame, final three frames show a run where the bed was initially at the bottom of the frame. From Anilkumar et al. (1993).

Figure 32. Late stages of lofting of a bed of glass beads initially at rest on a screen mesh, times ranging from 26 ms after flow initiation to 44 ms. Time between frames 1-9 approximately 1 ms; 9-14, 2 ms. From Anilkumar et al. (1993).

Figure 33. Contours of logarithm of particle volume fraction overlaid on velocity field, for a simulated eruption with a brief discharge that is turned off at 50 s. Plots are shown for times of 50, 70, and 100 s after eruption initation. From Valentine and Wohletz (1989).

Figure 34. Upwind stagnation point and displacement of plume axis in an eruption column. Arrows within the plume show velocity vectors in the spreading region. From Francis (1993).

Figure 35. Ratio of distance to stagnation point to axial displacement plotted against height of the base of the umbrella region, for crosswind speeds of 10, 20, and 30 m/s, illustrating different shapes of the eruption columns. From Carey and Sparks (1986).

Figure 36. Qualitative mixing diagram showing how ratio of magma and surface water intersected by eruption column affects eruption column dynamics. Note, vertical axis is mislabeled as "ground water" and should read "surface water." From Koyaguchi and Woods (1996).

Table 1. Definition of Variables

Symbol	Definition	Dimensions
c_d	drag coefficient	--------
c_v	specific heat at constant volume	$L^2T^{-2}K^{-1}$
d_p	particle or drop diameter	L
F	latent head production from vapor exsolution	$ML^{-1}T^{-3}$
g	gravitational acceleration	LT^{-2}
I	specific internal energy	L^2T^{-2}
K	interphase drag function	$ML^{-3}T^{-1}$
k	thermal conductivity	$MLT^{-3}K^{-1}$
M	molecular weight of air or water vapor	M/mole
Nu	Nusselt number	--------
p	pressure	$ML^{-1}T^{-2}$
Q	source of particles/drops from other populations	$ML^{-3}T^{-1}$
R	interphase heat transfer function	$ML^{-1}T^{-3}K^{-1}$
R_m	gas constant for mixture of gases	$L^2T^{-2}K^{-1}$
Re	Reynolds number	---------
T	temperature	K
t	time	T
u	velocity	LT^{-1}
ΔT_v	temperature difference between particles/drops and vapor	K
Δu_v	slip velocity between particle/drop field and vapor field	LT^{-1}
x	mole fraction air or water vapor in vapor field	---------
y	mass fraction of air or water vapor in vapor field	---------
Γ	vapor source from particles or drops	$ML^{-3}T^{-1}$
μ	viscosity	$ML^{-1}T^{-1}$
θ	volume fraction	---------
ρ	material density	ML^{-3}
τ	stress tensor	$ML^{-1}T^{-2}$

subscripts and indices

a	air
p	particle and drop field
q	total number of particle and drop populations
r	particle or drop population
v	vapor field
w	water vapor

Table 2. Effect of condensation on transport of water vapor by volcanic eruption columns erupted through both dry and wet atmospheres with a mass flux of 1.7×10^7 kg/s.*

	No condensation		Moderate condensation		Rapid condensation	
	dry	wet	dry	wet	dry	wet
Maximum height (km)	12.1	15.1	12.1	15.1	12.4	16.3
Fraction of total water from source	0.74	0.30	0.74	0.30	0.74	0.30
Fraction of total vapor condensed	0	0	0.02	0.02	0.81	0.90
Vapor flux at column top ($\times 10^4$ kg/s)	22.2	54.2	21.8	53.0	4.1	5.5

*Table 2 of Glaze et al. (in press).

Table 3. Predicted plume heights for volcanic columns in different settings.*

Atmosphere Used	Tropopause, km	NBH, km	H, km
60° January	9	8.7	11.5
60° July	10	8.0	11.0
45° January	10	8.7	11.6
U.S. Standard	11	9.1	12.3
30° January	12	9.9	13.3
45° July	13	8.7	12.5
30° July	15	8.9	13.2
15° annual average	16	9.6	13.4

*Table 2 of Glaze and Baloga (1996).

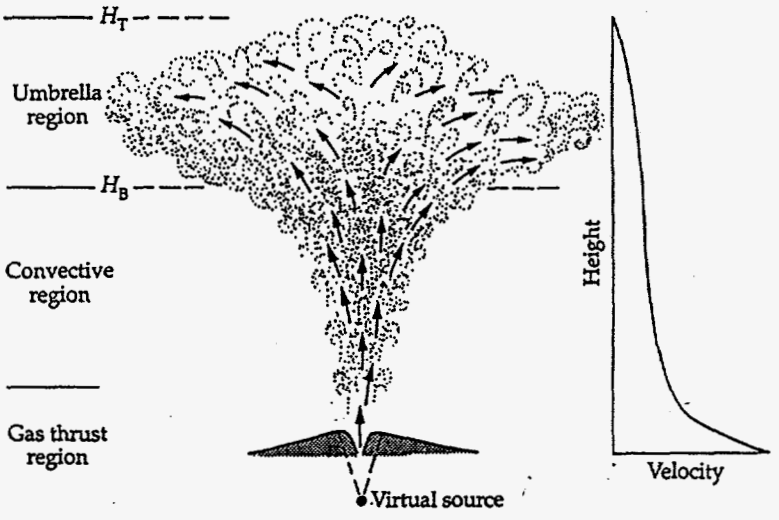
H_T
Umbrella region
H_B
Convective region
Gas thrust region
Virtual source
Height
Velocity

Fig. 2

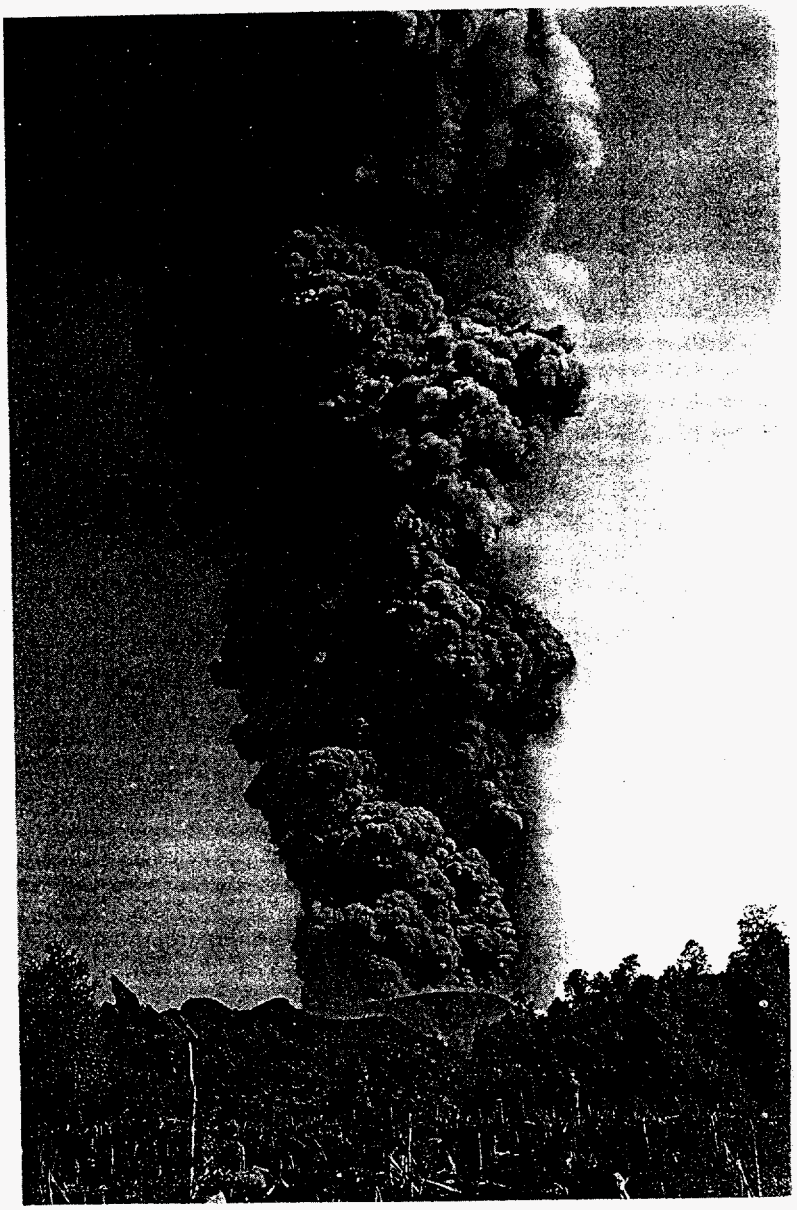

Ex. 2

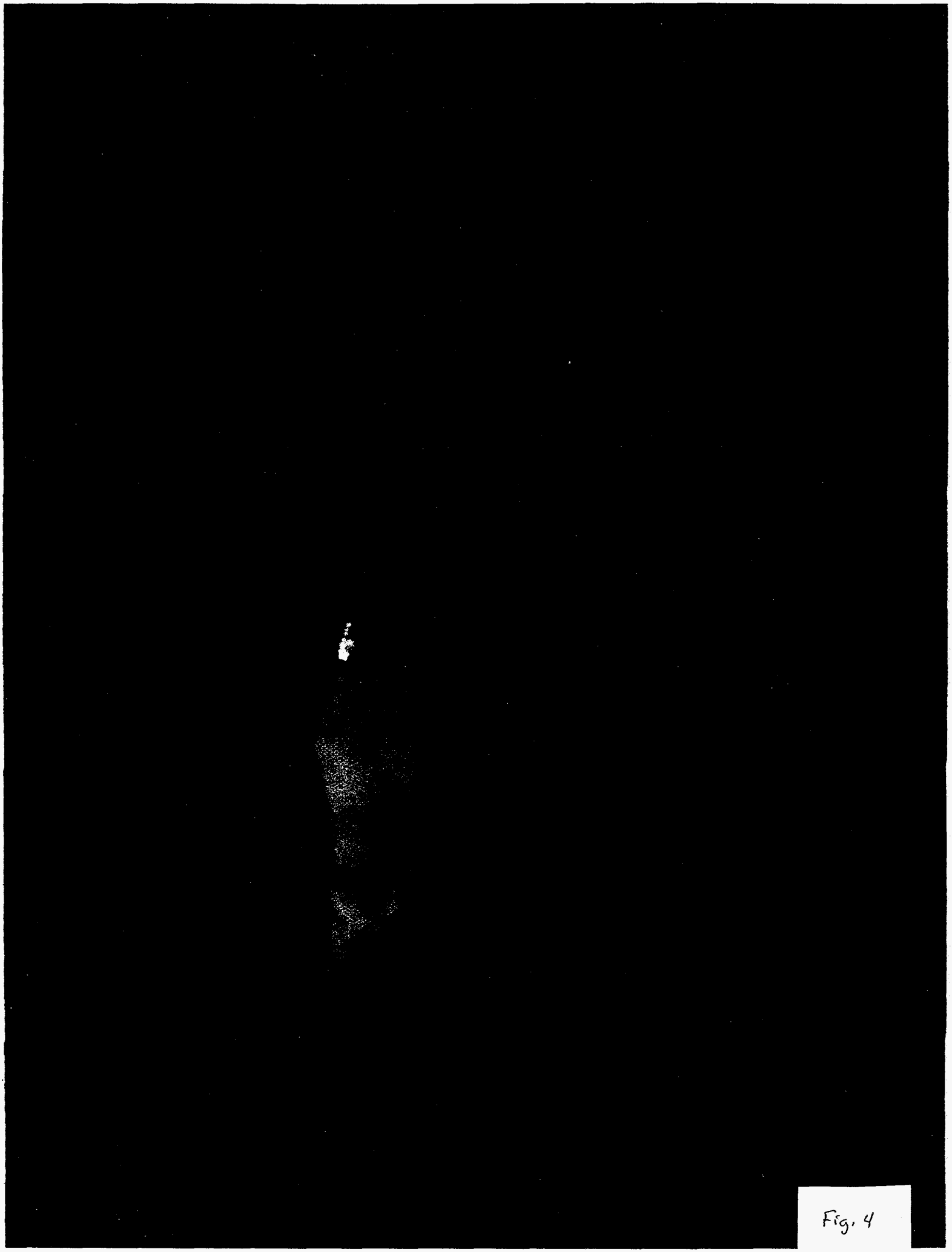

Fig. 4

THEORETICAL/NUMERICAL TREATMENTS - Basic conservation equations *fully describe all aspects of fluid flow.*

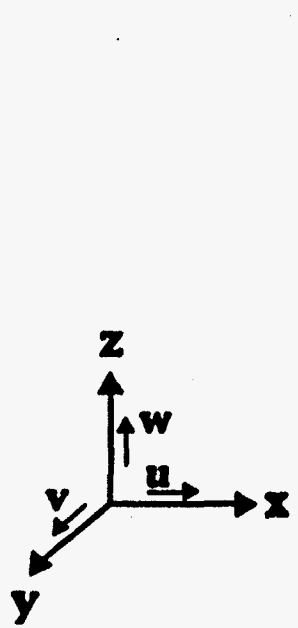

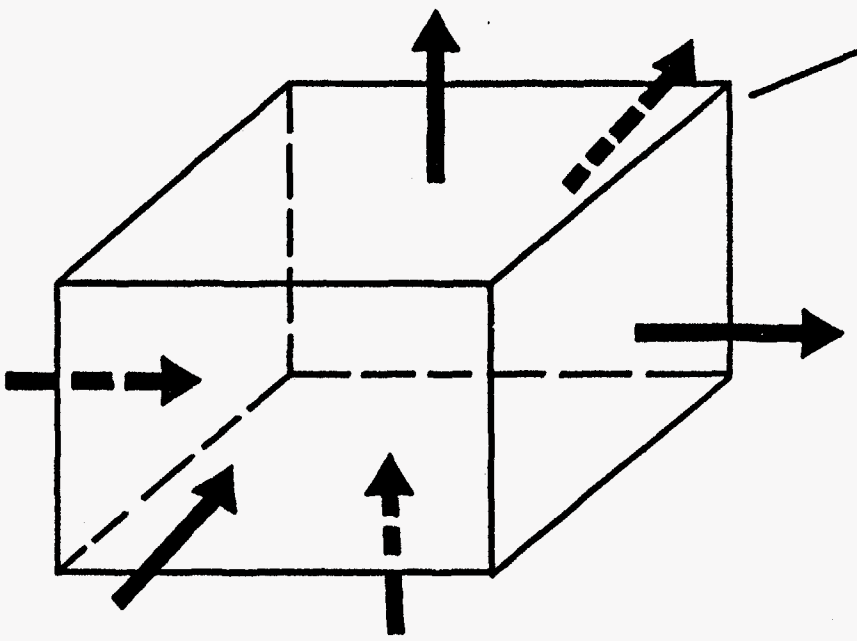

Control Volume

Flow of quantity Q through control volume.

Q = mass
momentum
energy

(change in Q with time) = (Q in) − (Q out) + (source of Q)

$$\frac{\partial Q}{\partial t} = -\left[\frac{\partial Qu}{\partial x} + \frac{\partial Qv}{\partial y} + \frac{\partial Qw}{\partial z}\right] + \text{source terms}$$

Fig. 5

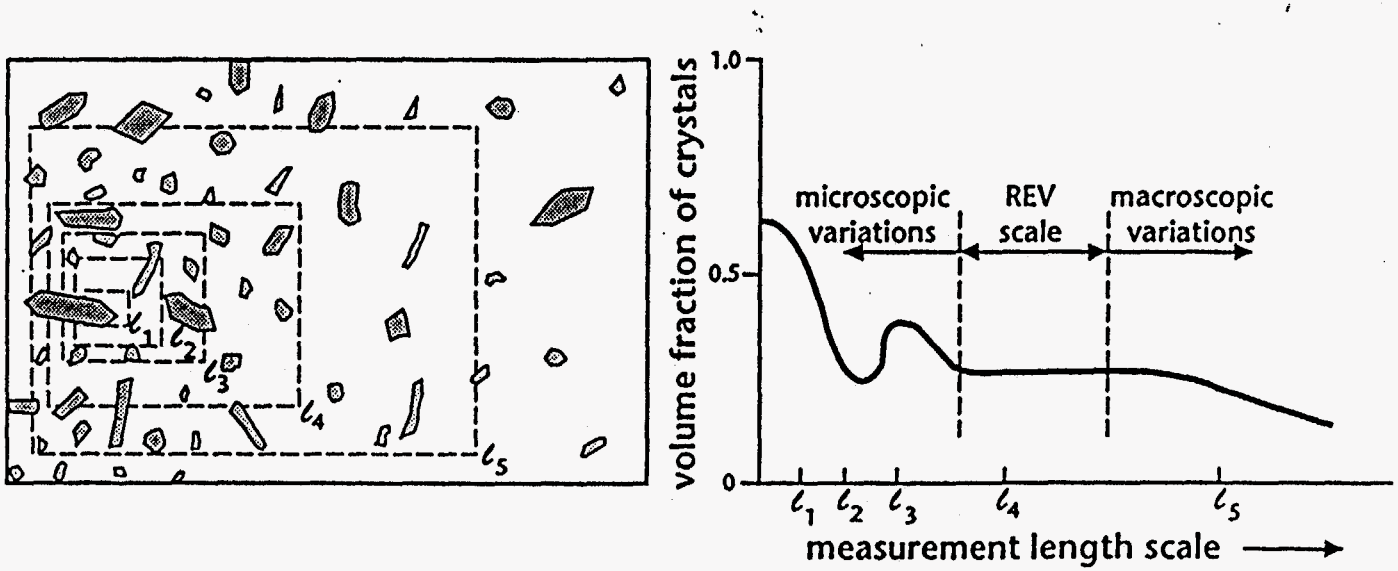
volume fraction of crystals
1.0
0.5
0
microscopic variations
REV scale
macroscopic variations
ℓ_1 ℓ_2 ℓ_3 ℓ_4 ℓ_5
measurement length scale

Fig. 6

EFFECT OF MACH NUMBER ON TURBULENCE AND ENTRAINMENT

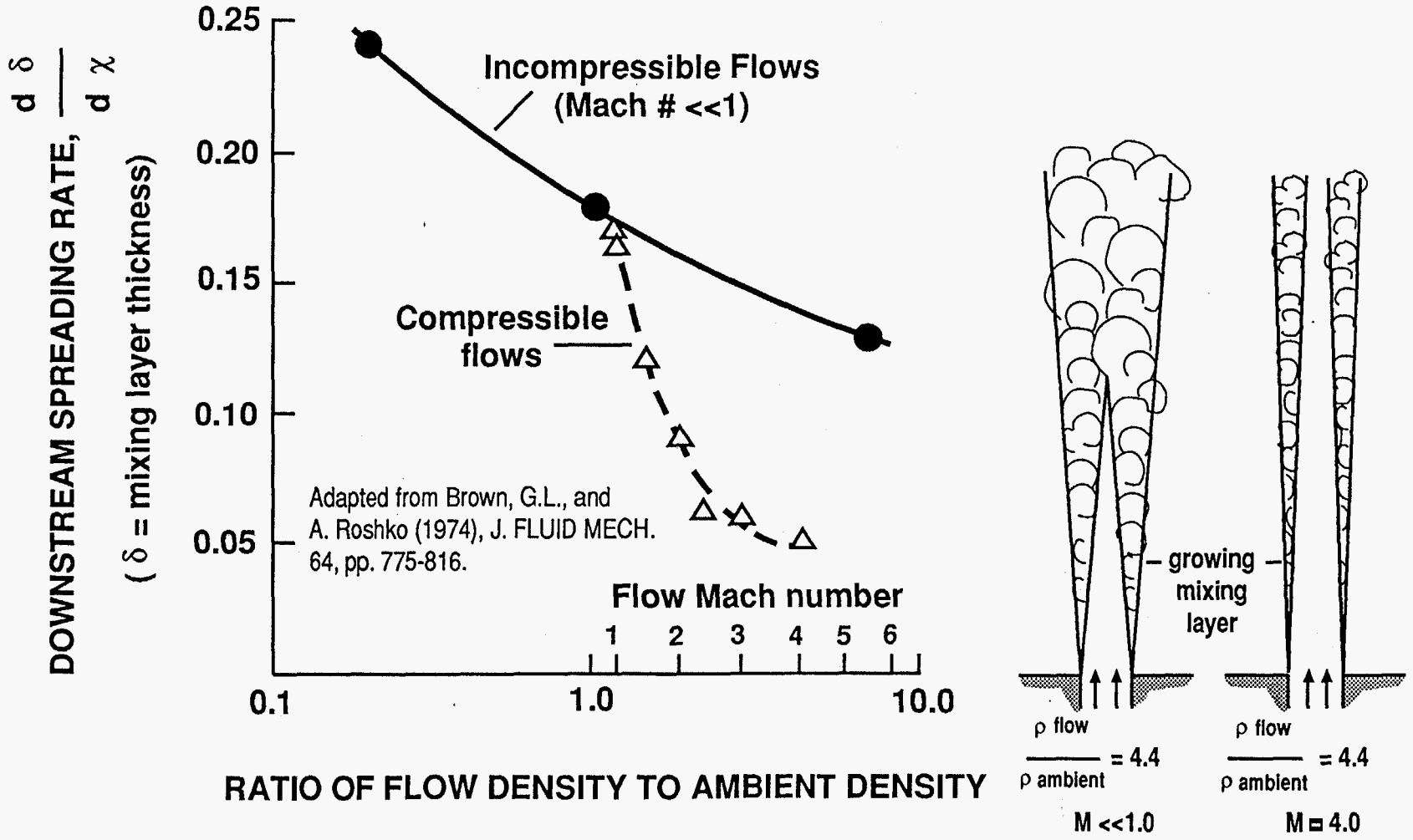

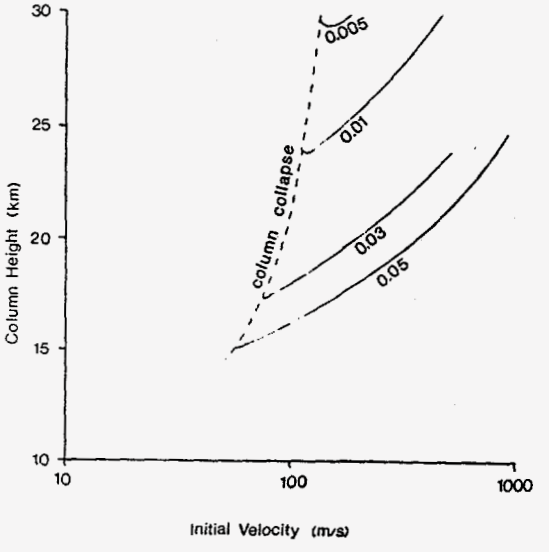
30
25
20
15
10
Column Height (km)
0.005
0.01
column collapse
0.03
0.05
10
100
1000
Initial Velocity (m/s)

a

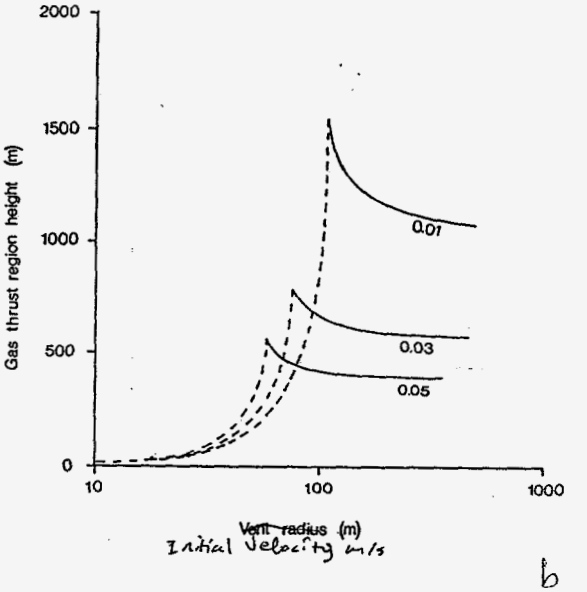
2000
1500
1000
500
0
Gas thrust region height (m)
0.01
0.03
0.05
10
100
1000
Vent radius (m)
Initial Velocity m/s

b

182

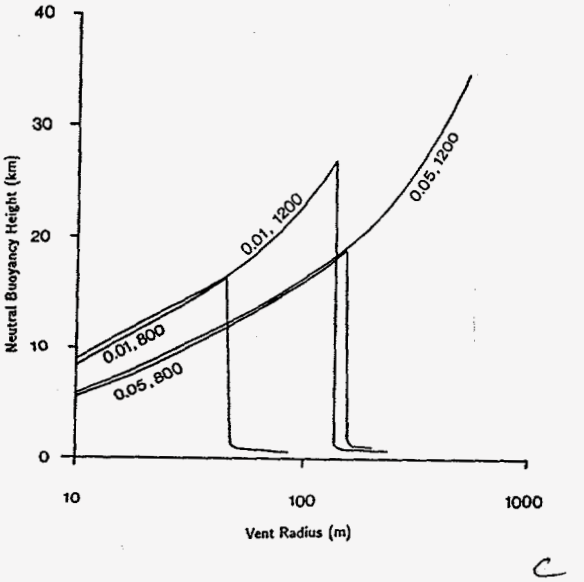
40
30
20
10
0
Neutral Buoyancy Height (km)
0.01, 1200
0.05, 1200
0.01, 800
0.05, 800
10
100
1000
Vent Radius (m)

c

Fig. 8

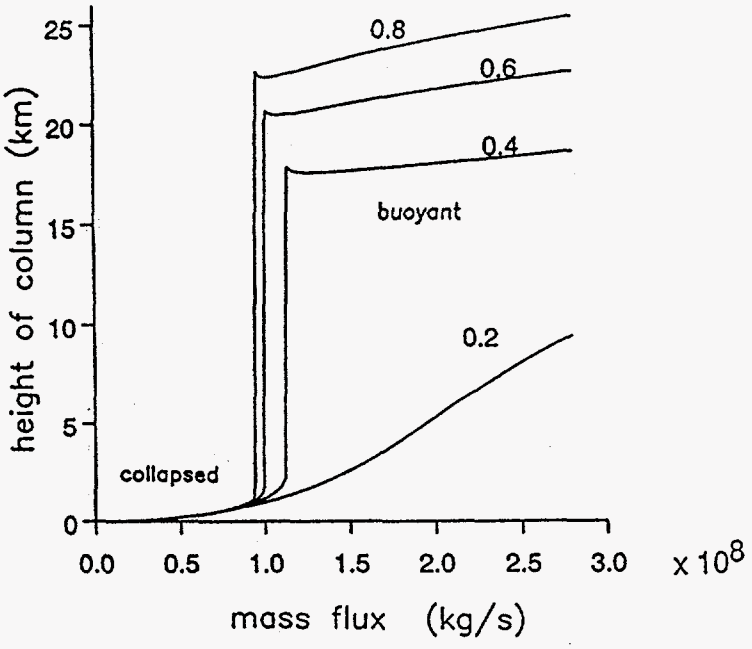
height of column (km)
25
20
15
10
5
0
0.8
0.6
0.4
buoyant
0.2
collapsed
0.0
0.5
1.0
1.5
2.0
2.5
3.0
x 10^8
mass flux (kg/s)

Fig. 9

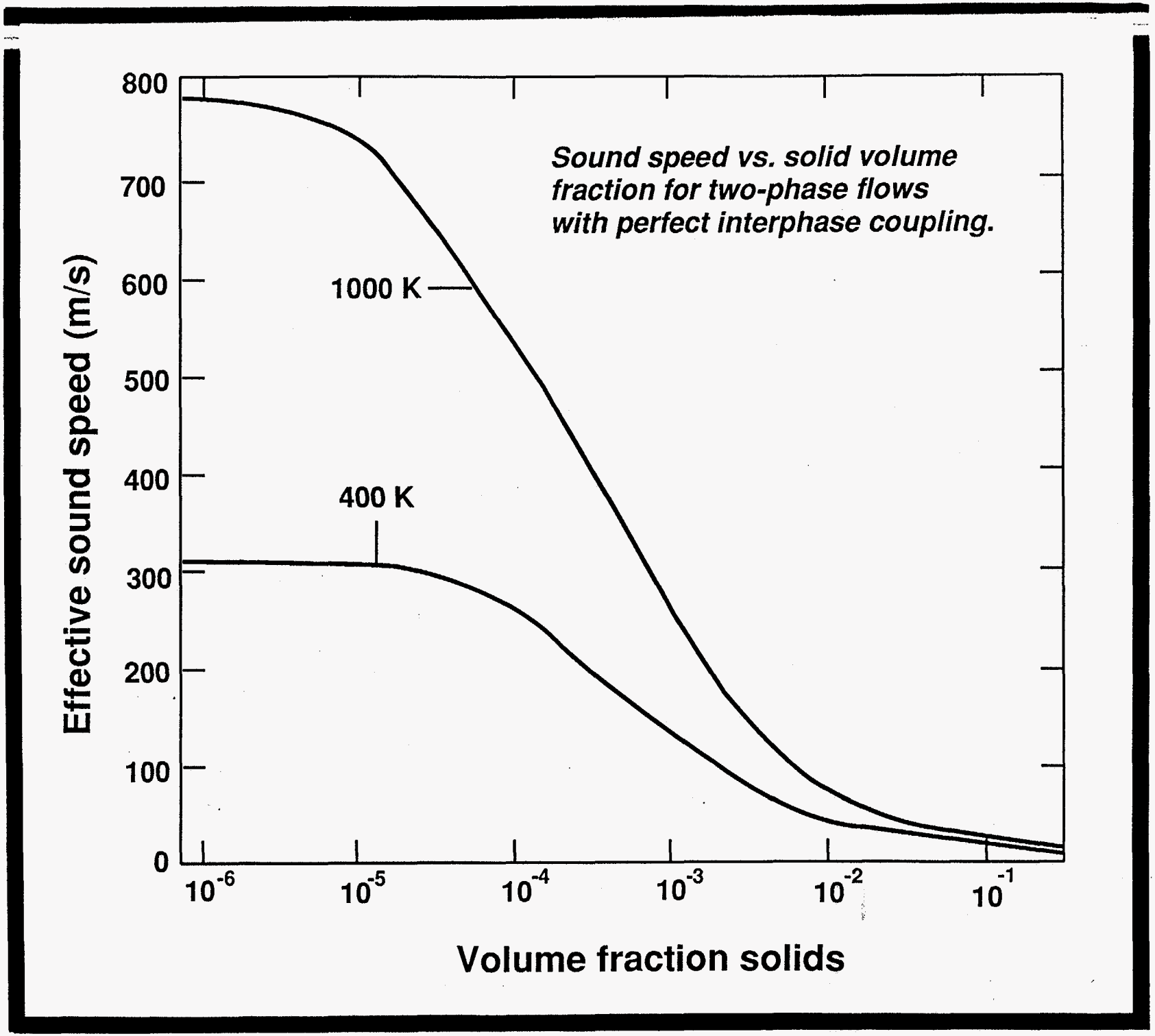
Sound speed vs. solid volume fraction for two-phase flows with perfect interphase coupling.
1000 K
400 K
Effective sound speed (m/s)
800
700
600
500
400
300
200
100
0
10^{-6}
10^{-5}
10^{-4}
10^{-3}
10^{-2}
10^{-1}
Volume fraction solids

Fig 10

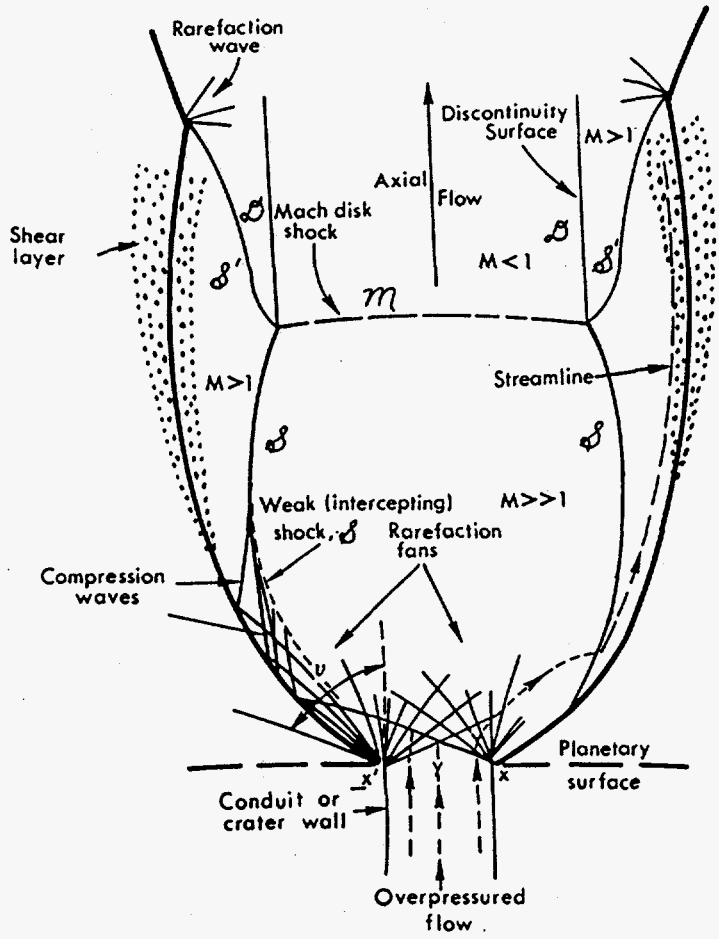
Rarefaction wave
Discontinuity Surface
M>1
Axial Flow
Mach disk shock
Shear layer
M<1
m
M>1
Streamline
Weak (intercepting) shock
M>>1
Rarefaction fans
Compression waves
Planetary surface
Conduit or crater wall
Overpressured flow

Frg. 11

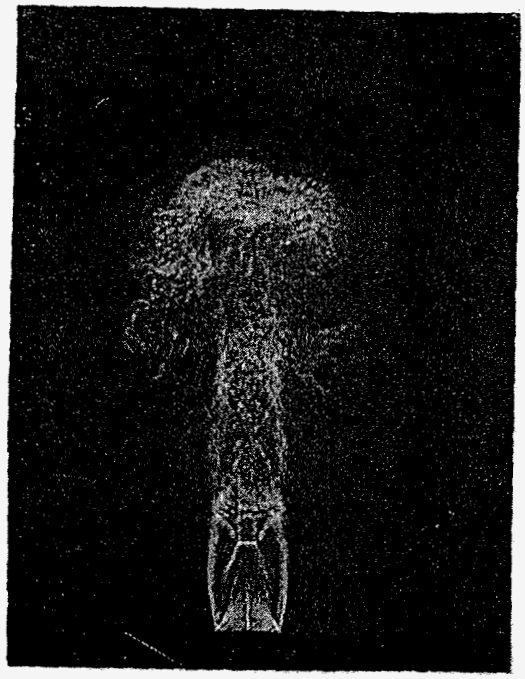

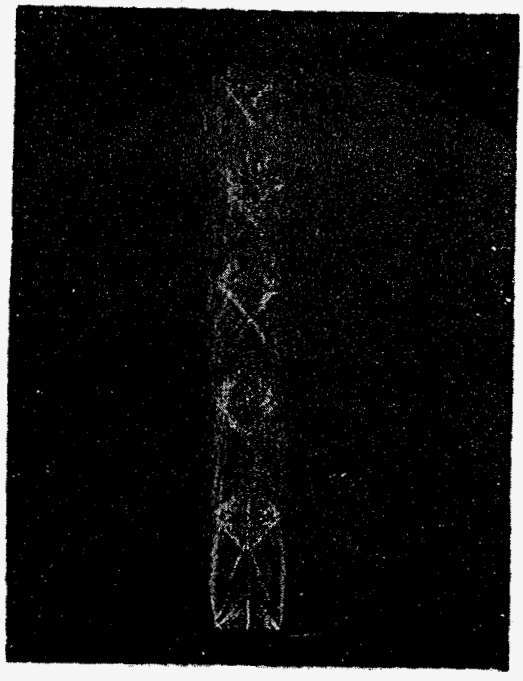

Fig. 12

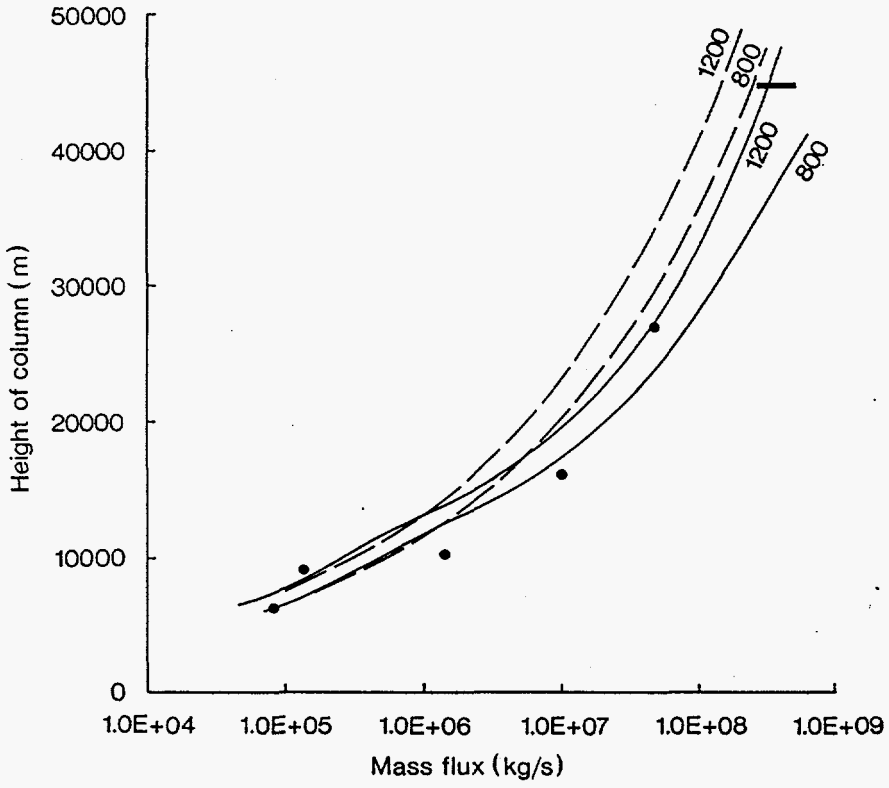
50000
40000
30000
20000
10000
0
Height of column (m)
1.0E+04
1.0E+05
1.0E+06
1.0E+07
1.0E+08
1.0E+09
Mass flux (kg/s)
1200
800
1200
800

Fig. 13

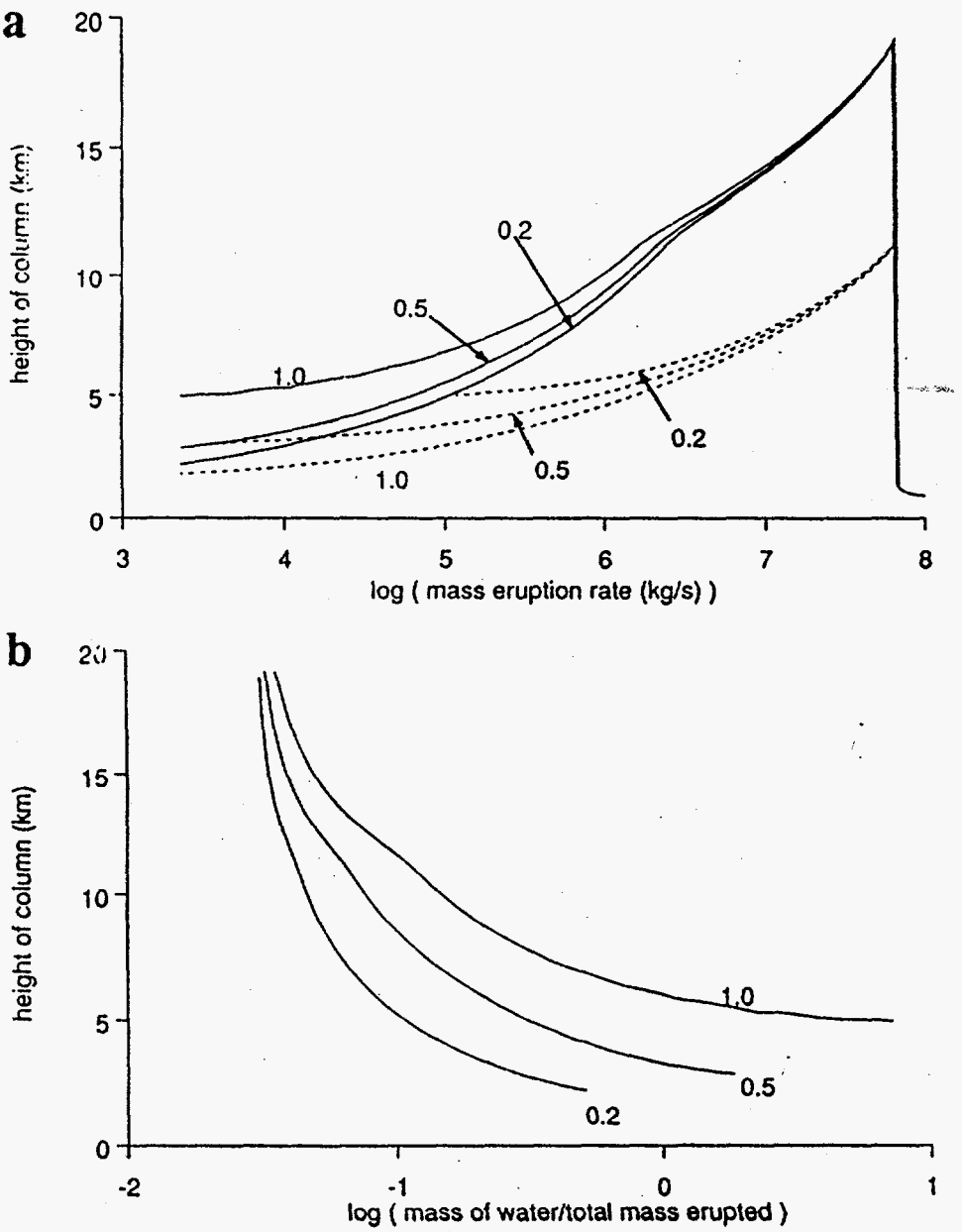
a
height of column (km)
20
15
10
5
0
3
4
5
6
7
8
log (mass eruption rate (kg/s))
0.2
0.5
1.0
1.0
0.5
0.2
b
height of column (km)
20
15
10
5
0
-2
-1
0
1
log (mass of water/total mass erupted)
1.0
0.5
0.2

Fig. 14

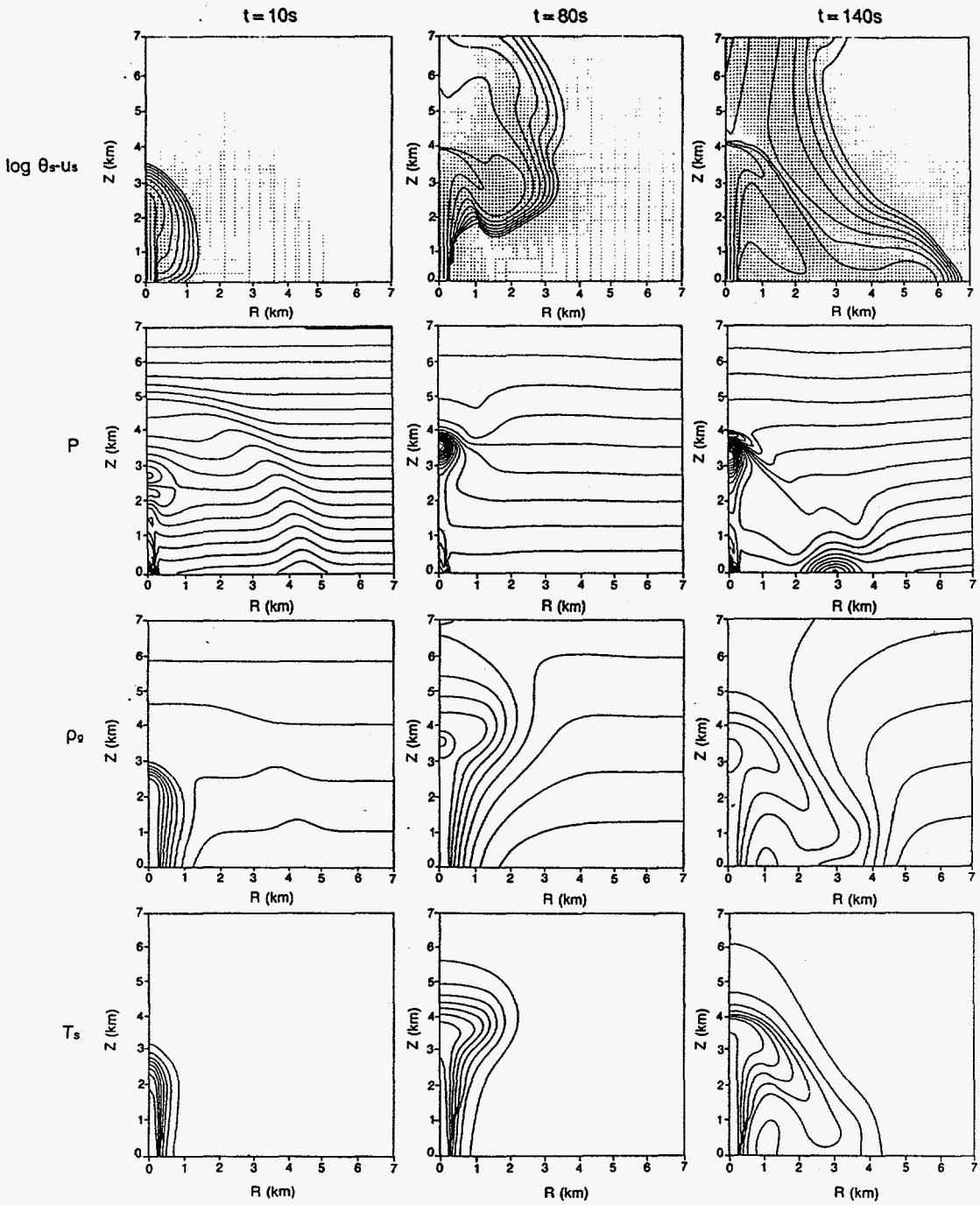

Fig 15

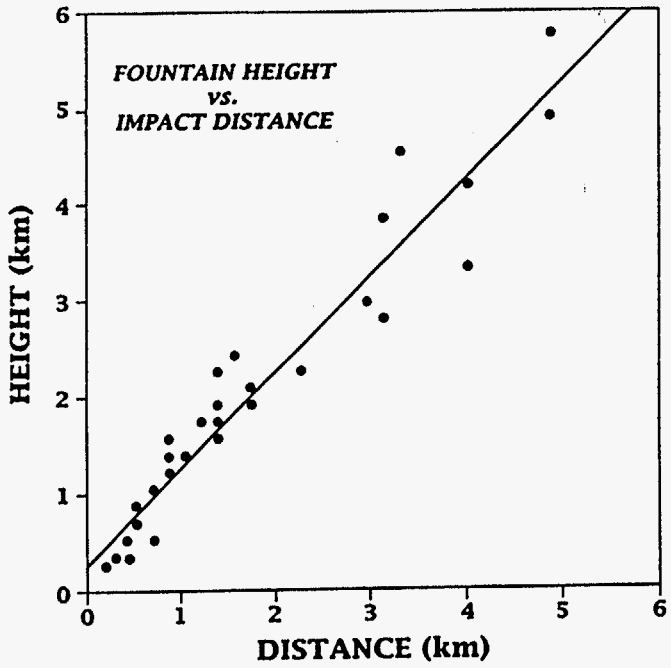
FOUNTAIN HEIGHT
vs.
IMPACT DISTANCE
HEIGHT (km)
DISTANCE (km)
0
1
2
3
4
5
6

Fig. 16

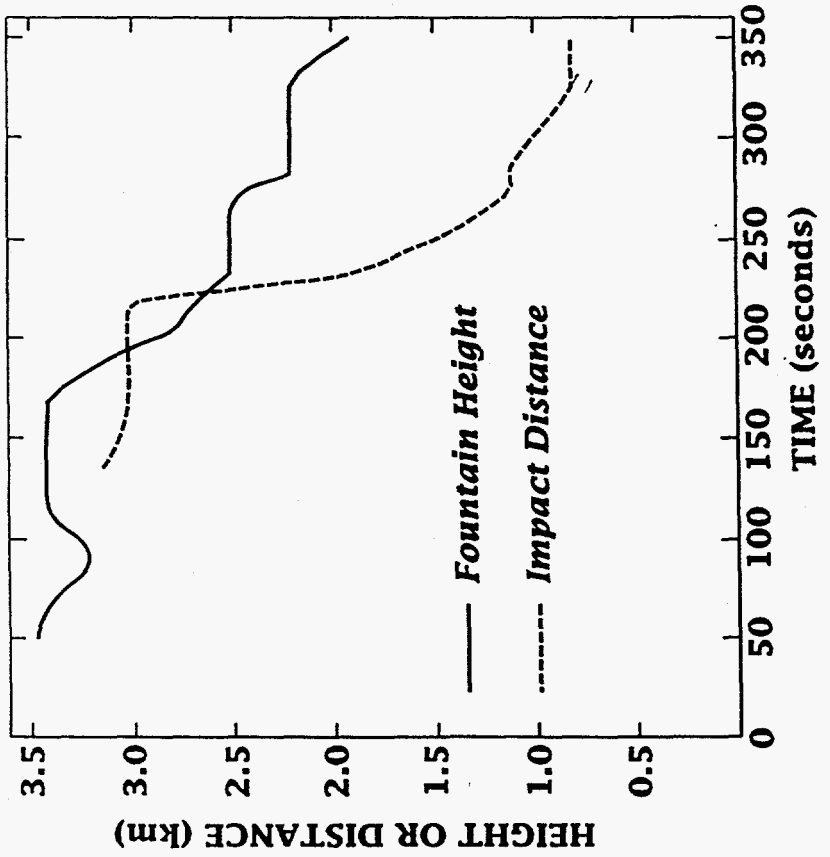
HEIGHT OR DISTANCE (km)
3.5
3.0
2.5
2.0
1.5
1.0
0.5
0
50
100
150
200
250
300
350
TIME (seconds)
Fountain Height
Impact Distance

Fig. 17

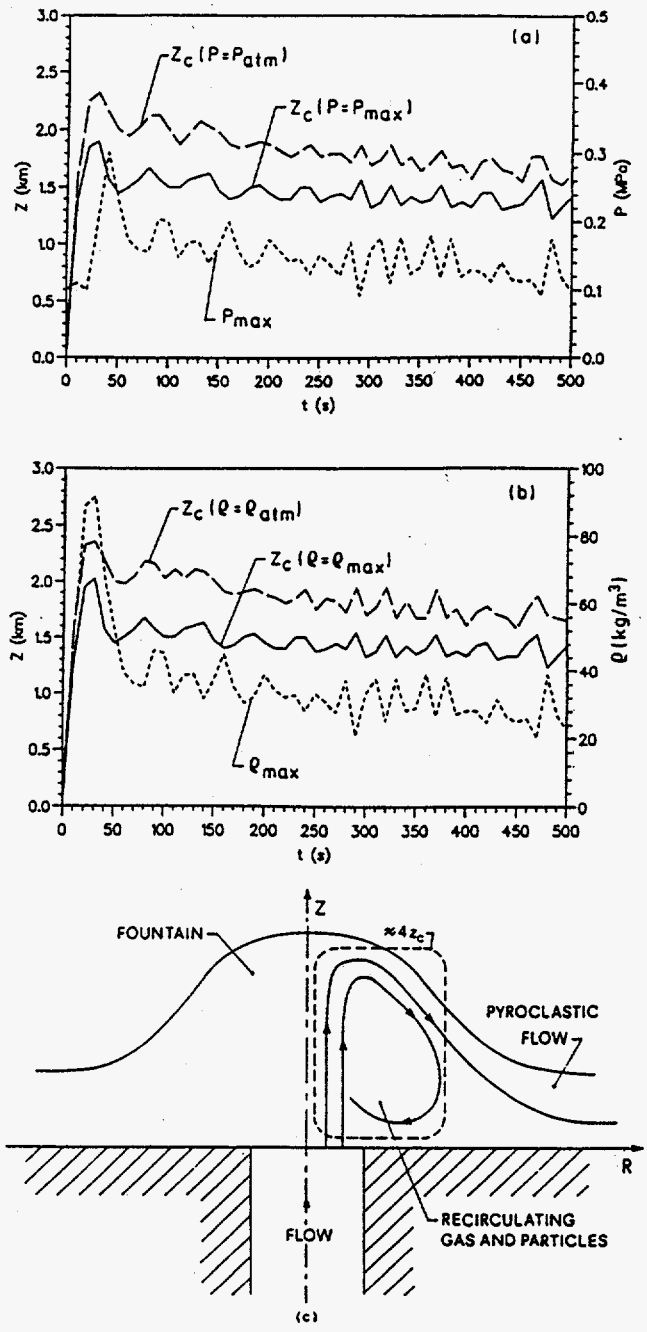
(a)
$Z_c (P=P_{atm})$
$Z_c (P=P_{max})$
P_{max}
Z (km)
P (MPa)
t (s)
(b)
$Z_c (\varrho=\varrho_{atm})$
$Z_c (\varrho=\varrho_{max})$
ϱ_{max}
Z (km)
ϱ (kg/m^3)
t (s)
Z
FOUNTAIN
$\approx 4 z_c$
PYROCLASTIC FLOW
R
FLOW
RECIRCULATING GAS AND PARTICLES
(c)

Fig. 18

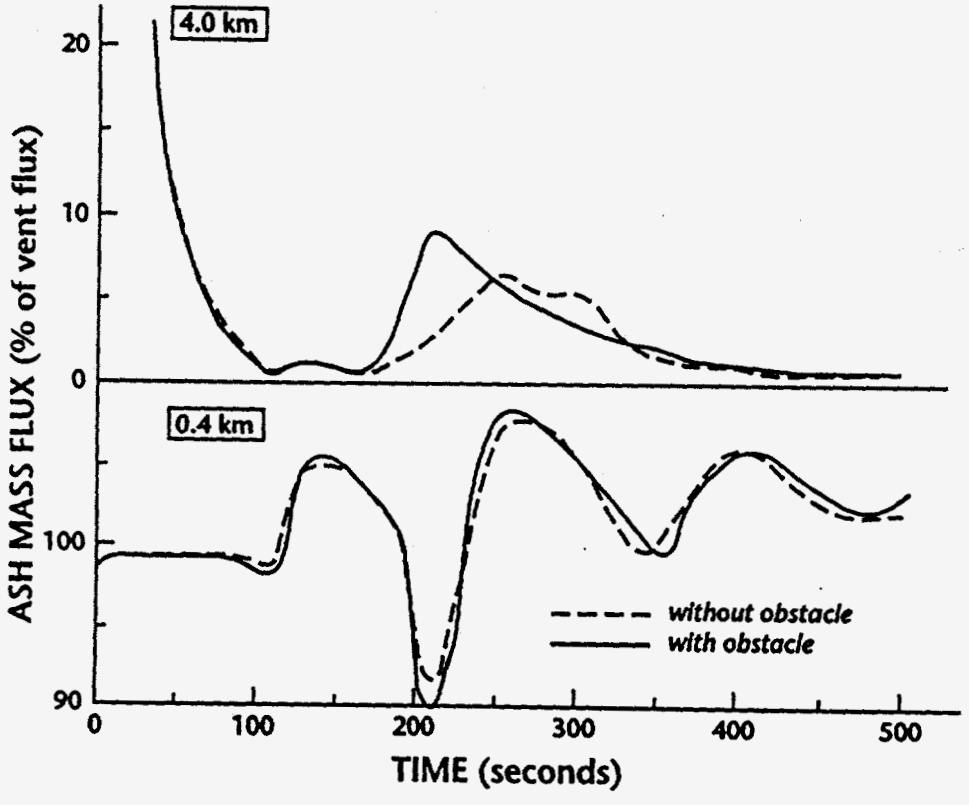
4.0 km
0.4 km
20
10
0
100
90
ASH MASS FLUX (% of vent flux)
0
100
200
300
400
500
TIME (seconds)
without obstacle
with obstacle

Fig. 19

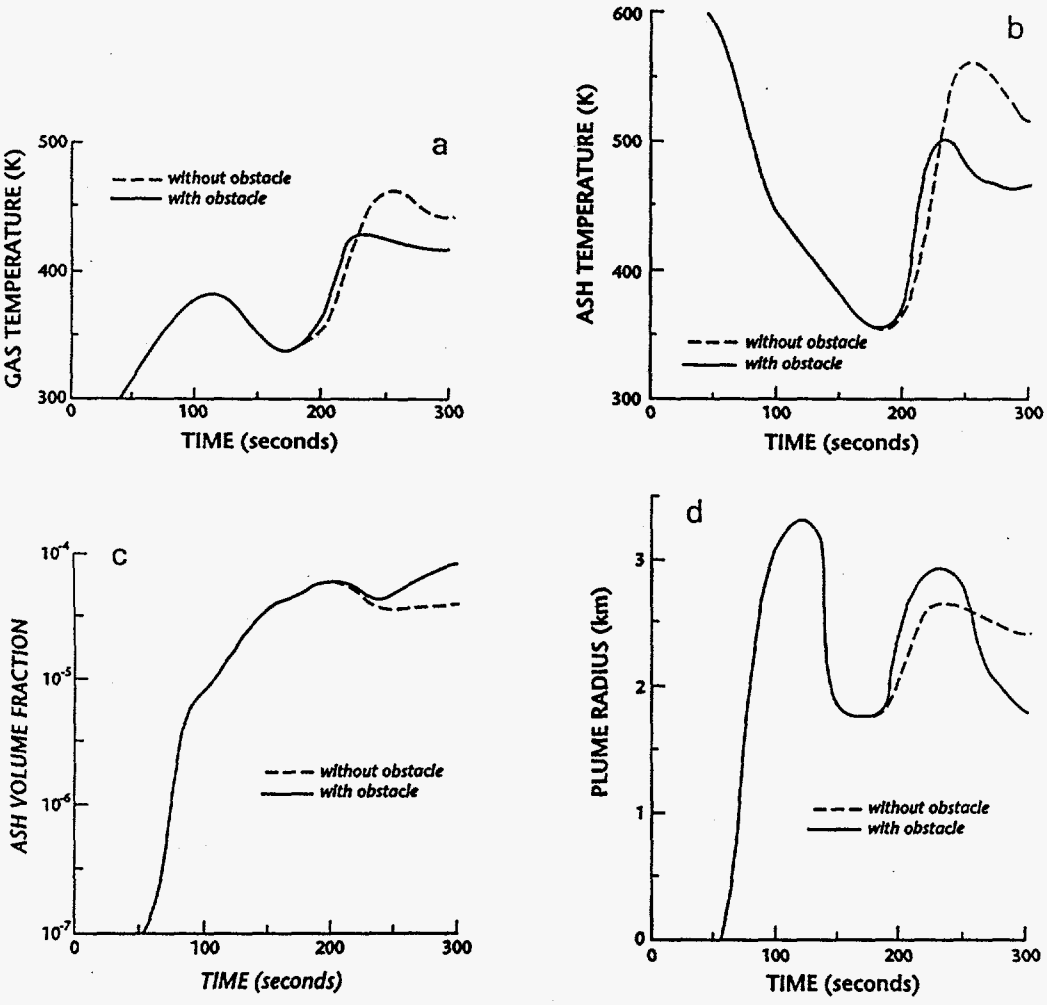
a
GAS TEMPERATURE (K)
500
400
300
0
100
200
300
TIME (seconds)
without obstacle
with obstacle
b
ASH TEMPERATURE (K)
600
500
400
300
0
100
200
300
TIME (seconds)
without obstacle
with obstacle
c
ASH VOLUME FRACTION
10^{-4}
10^{-5}
10^{-6}
10^{-7}
0
100
200
300
TIME (seconds)
without obstacle
with obstacle
d
PLUME RADIUS (km)
3
2
1
0
0
100
200
300
TIME (seconds)
without obstacle
with obstacle

Fig. 20

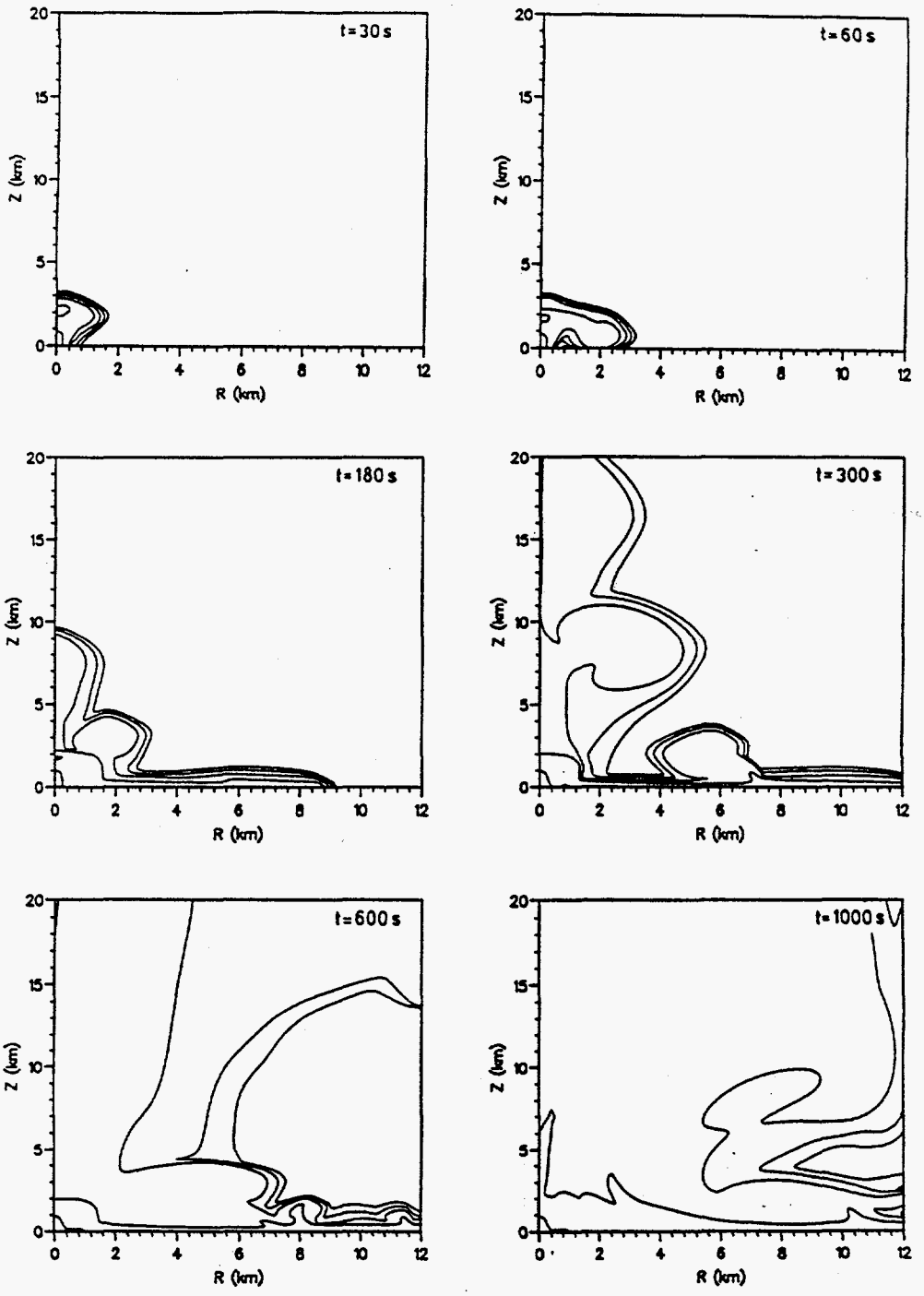
t=30 s
t=60 s
t=180 s
t=300 s
t=600 s
t=1000 s
Z (km)
R (km)
0
5
10
15
20
0
2
4
6
8
10
12

Fig. 21

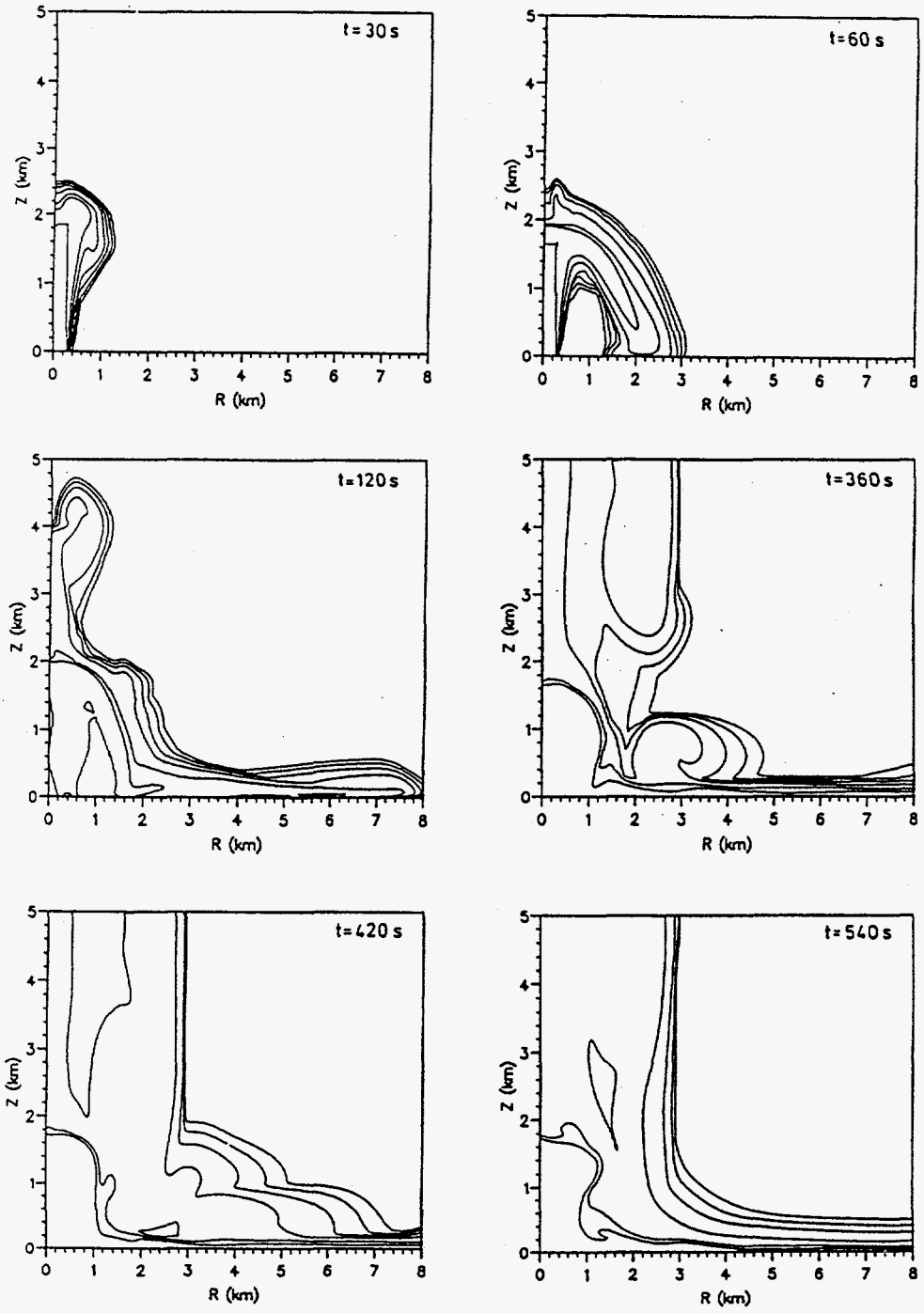

Fig. 22

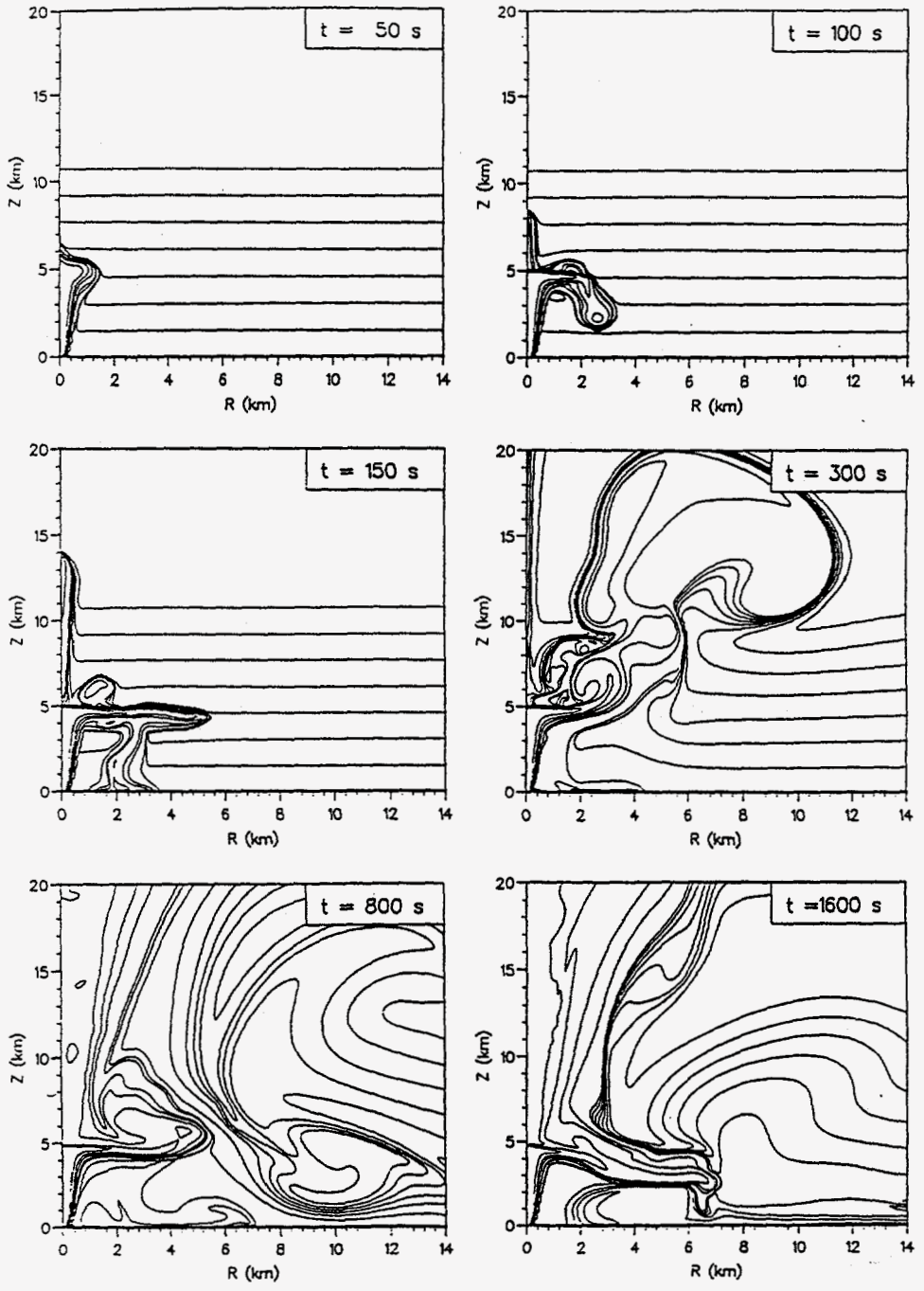
t = 50 s
t = 100 s
t = 150 s
t = 300 s
t = 800 s
t =1600 s
Z (km)
R (km)
0
5
10
15
20
0
2
4
6
8
10
12
14

Fig. 23

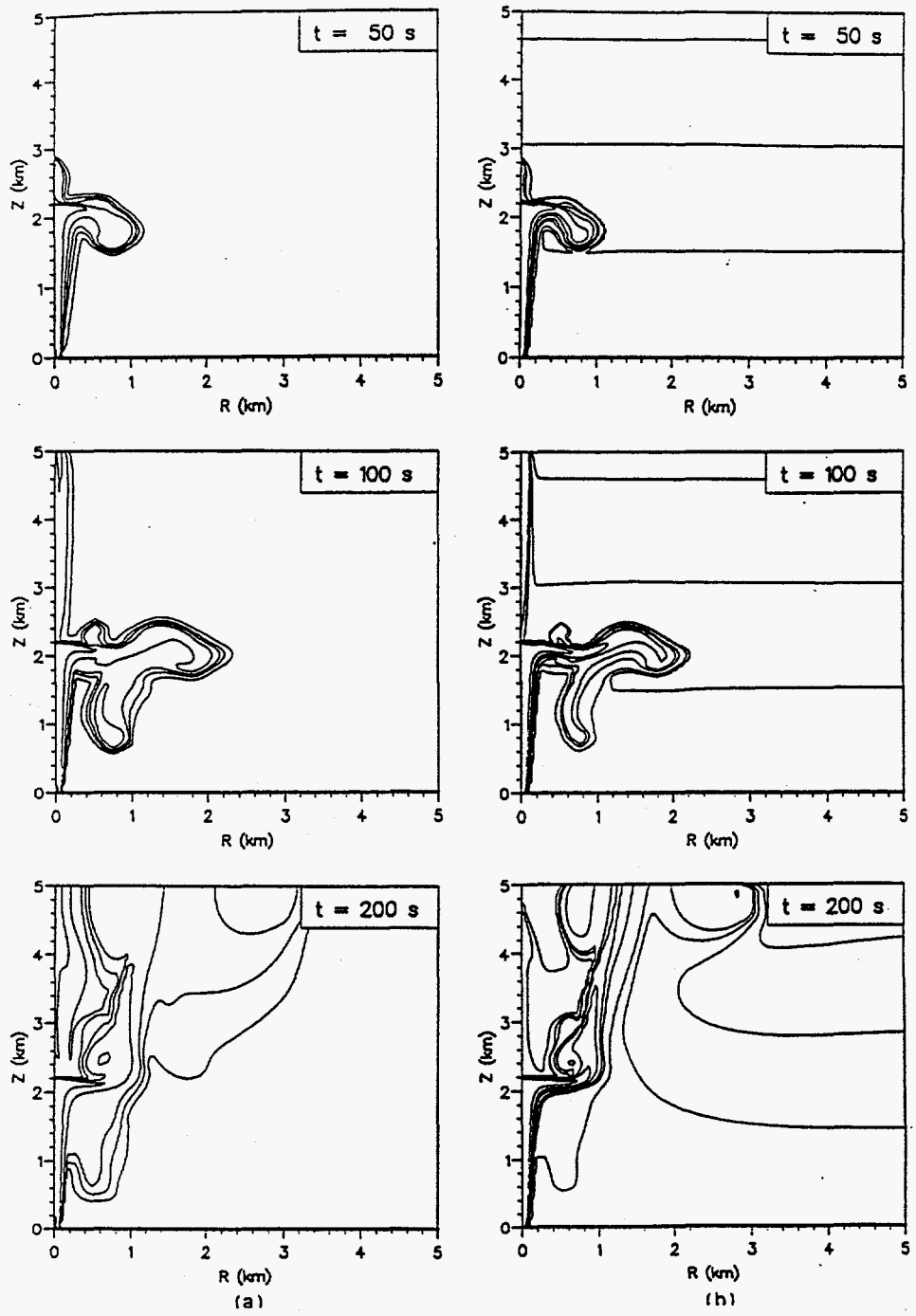

Fig. 24

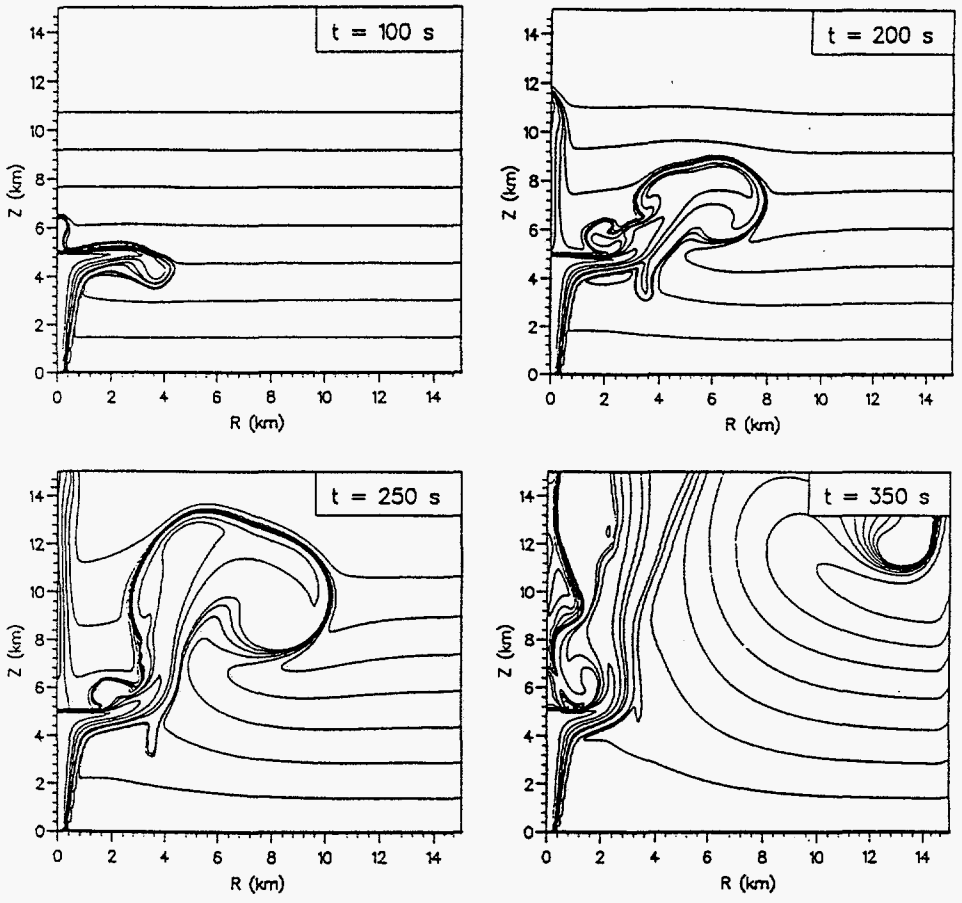

Fig. 25

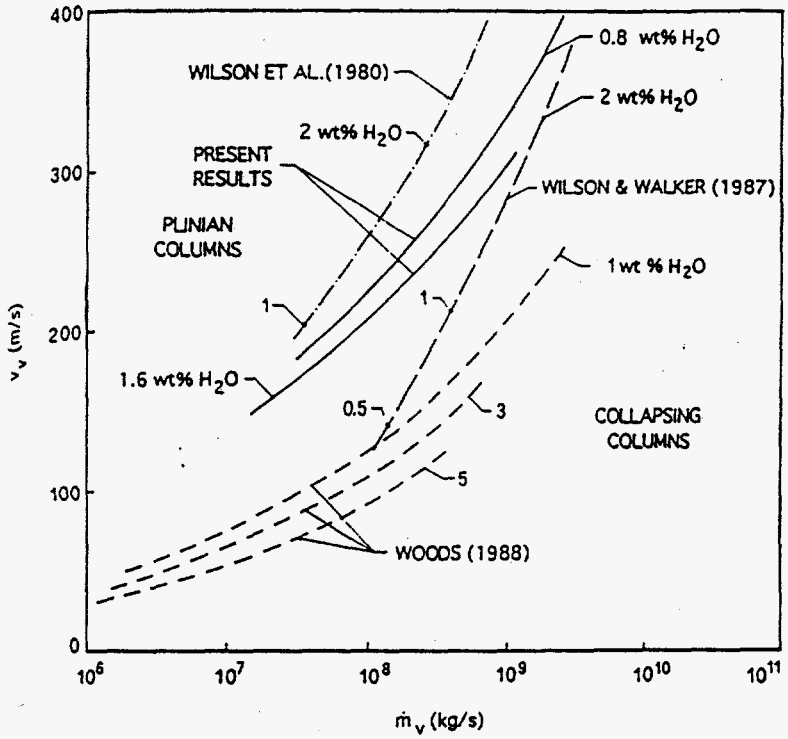
400
300
200
100
0
v_v (m/s)
WILSON ET AL.(1980)
2 wt% H_2O
PRESENT RESULTS
PLINIAN COLUMNS
1
1.6 wt% H_2O
0.8 wt% H_2O
2 wt% H_2O
WILSON & WALKER (1987)
1 wt % H_2O
1
0.5
3
5
COLLAPSING COLUMNS
WOODS (1988)
10^6
10^7
10^8
10^9
10^{10}
10^{11}
$\dot{m}_v$ (kg/s)

Fig. 26

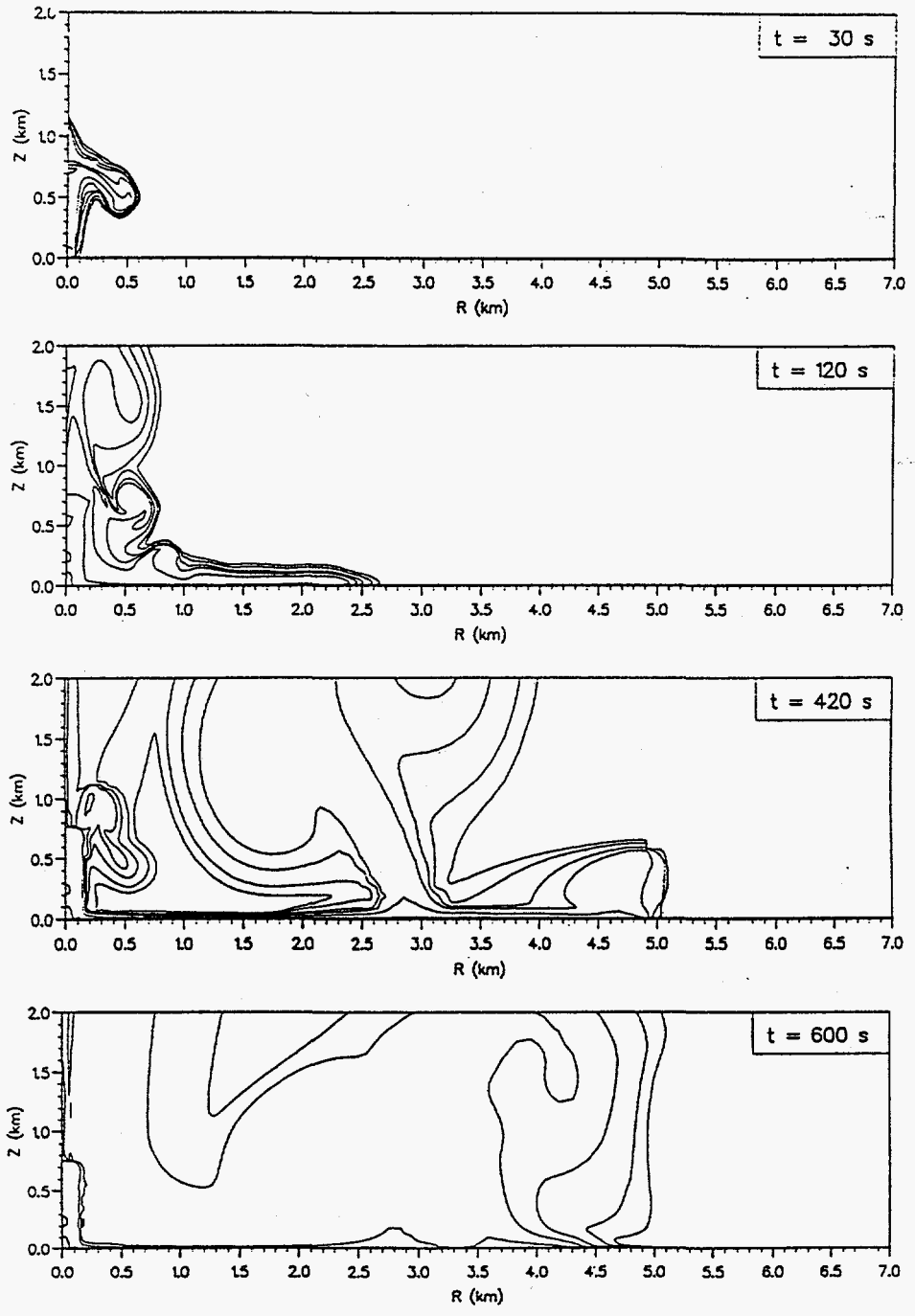

Distribution of particulate volumetric fraction in the atmosphere at 30, 120, 420, and 600 s of eruption *A1*. The contour levels shown are the exponents to the base 10 and, beginning from the outer or distant from the vent region, correspond to -10, -8, -6, -5, -4, -3, -2, and -1.

Fig. 27

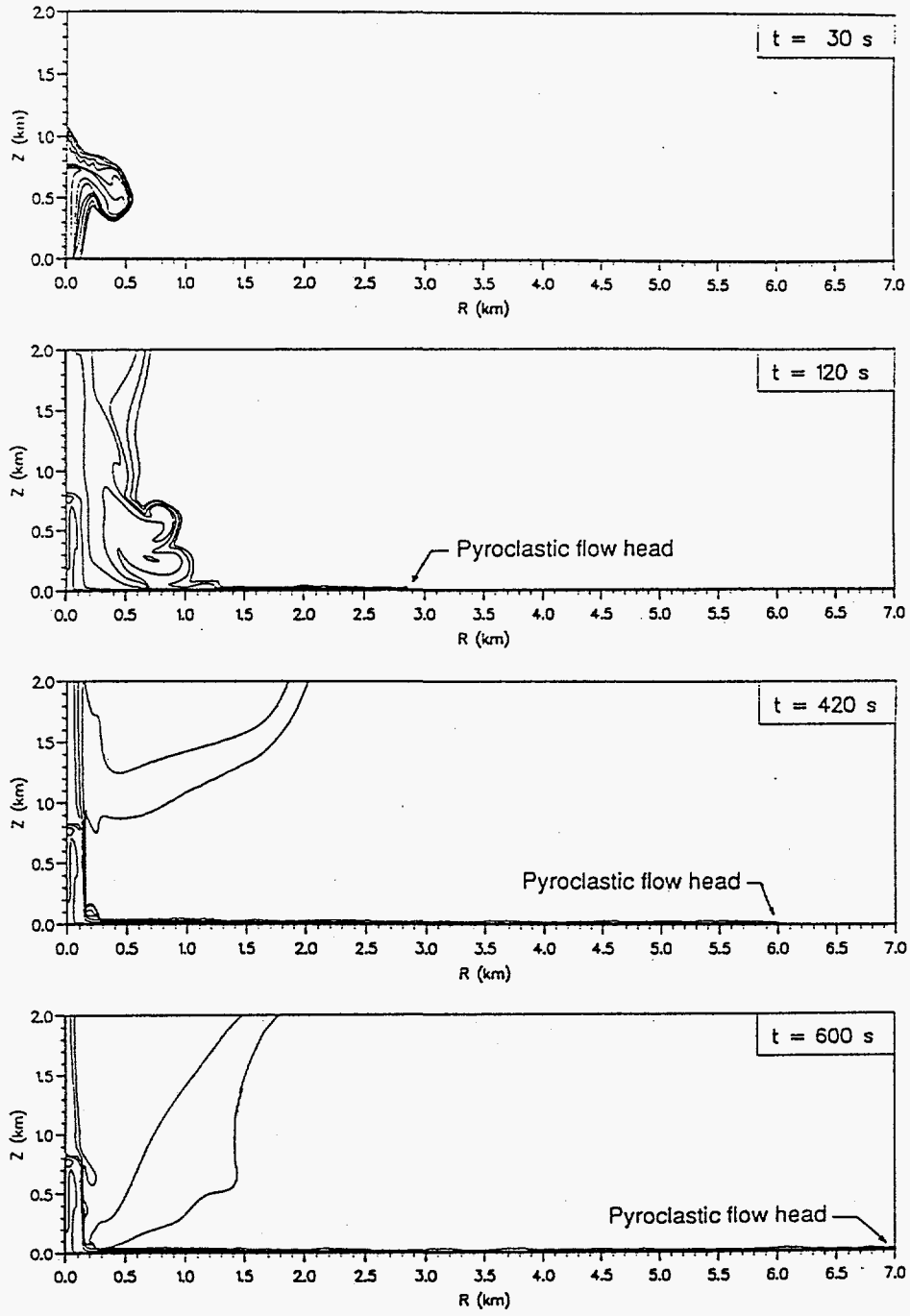

Distribution of particulate volumetric fraction in the atmosphere at 30, 120, 420, and 600 s of eruption *A2*. The contour levels shown are the exponents to the base 10 and, beginning from the outer or distant from the vent region, correspond to -10, -8, -6, -5, -4, -3, -2, and -1.

Fig. 28

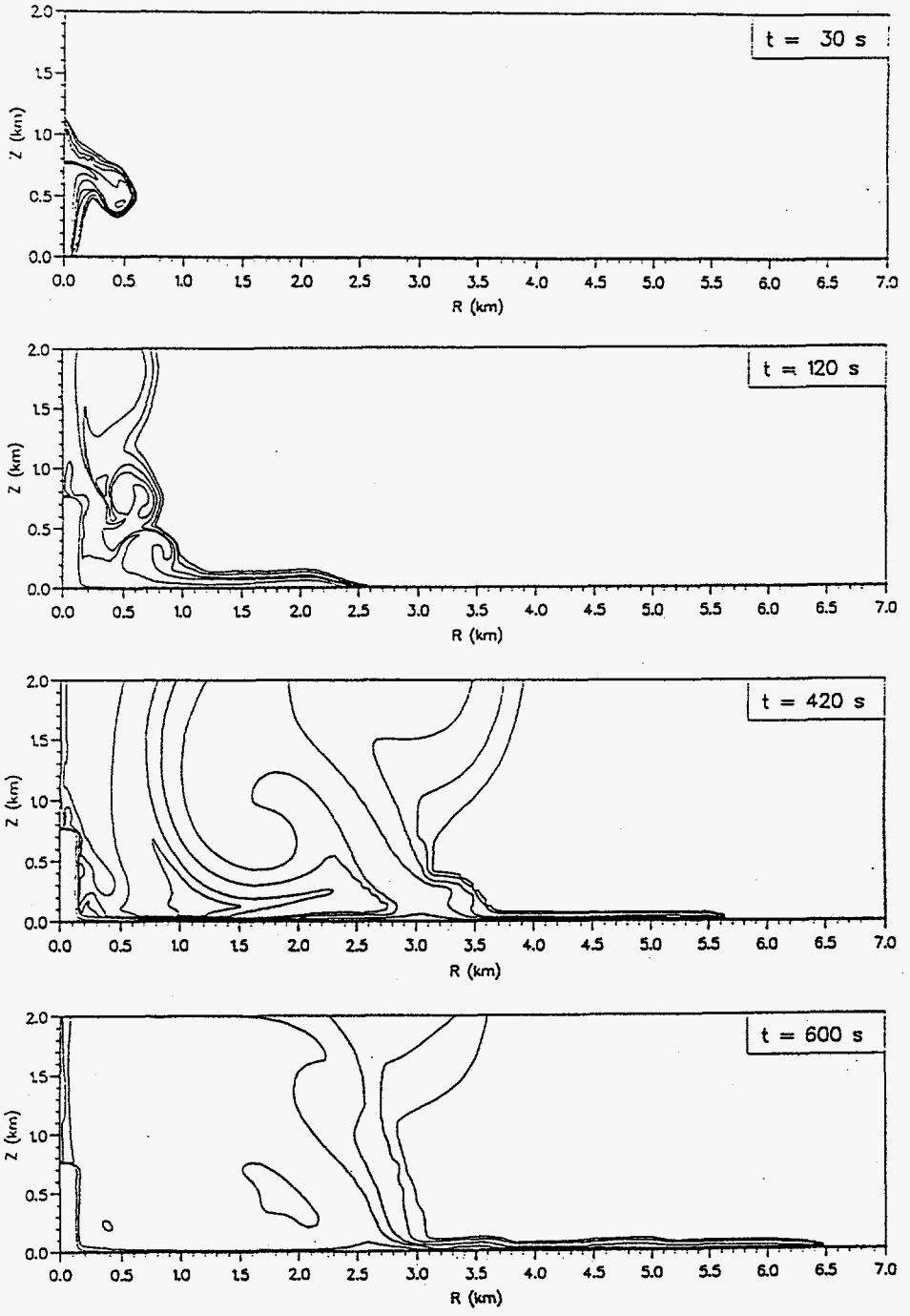

Distribution of solid volumetric fraction of particulate phase 1 ($d_{p1} = 10$ μm) at 30, 120, 420, and 600 s of eruption *A3*. The contour levels shown are the exponents to the base 10 and, beginning from the outer or distant from the vent region, correspond to -10, -8, -6, -5, -4, -3, -2, and -1.

Fig. 29

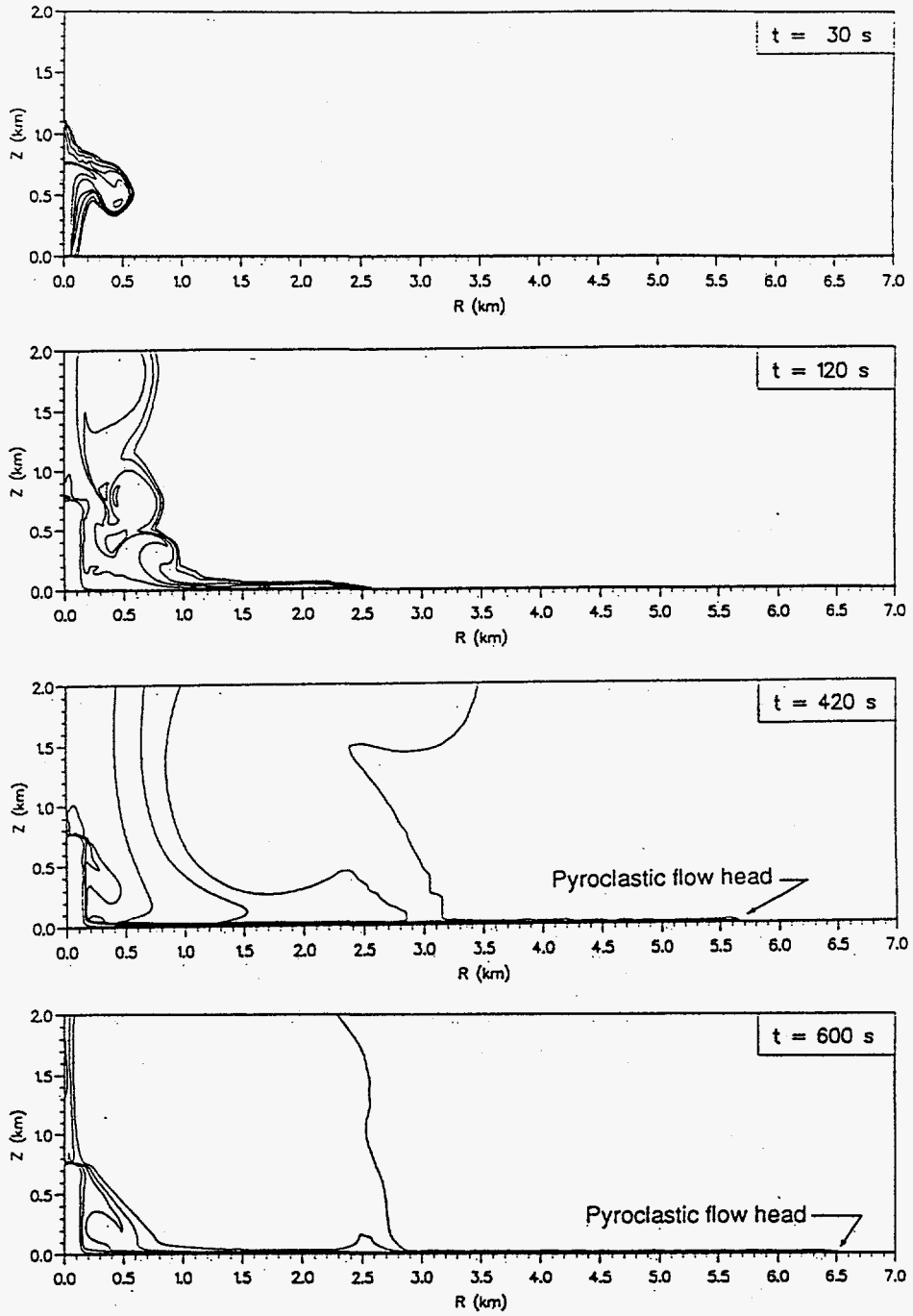

Distribution of solid volumetric fraction of particulate phase 2 ($d_{p2} = 200$ μm) at 30, 120, 420, and 600 s of eruption *A3*. The contour levels shown are the exponents to the base 10 and, beginning from the outer or distant from the vent region, correspond to -10, -8, -6, -5, -4, -3, -2, and -1.

Fig. 30

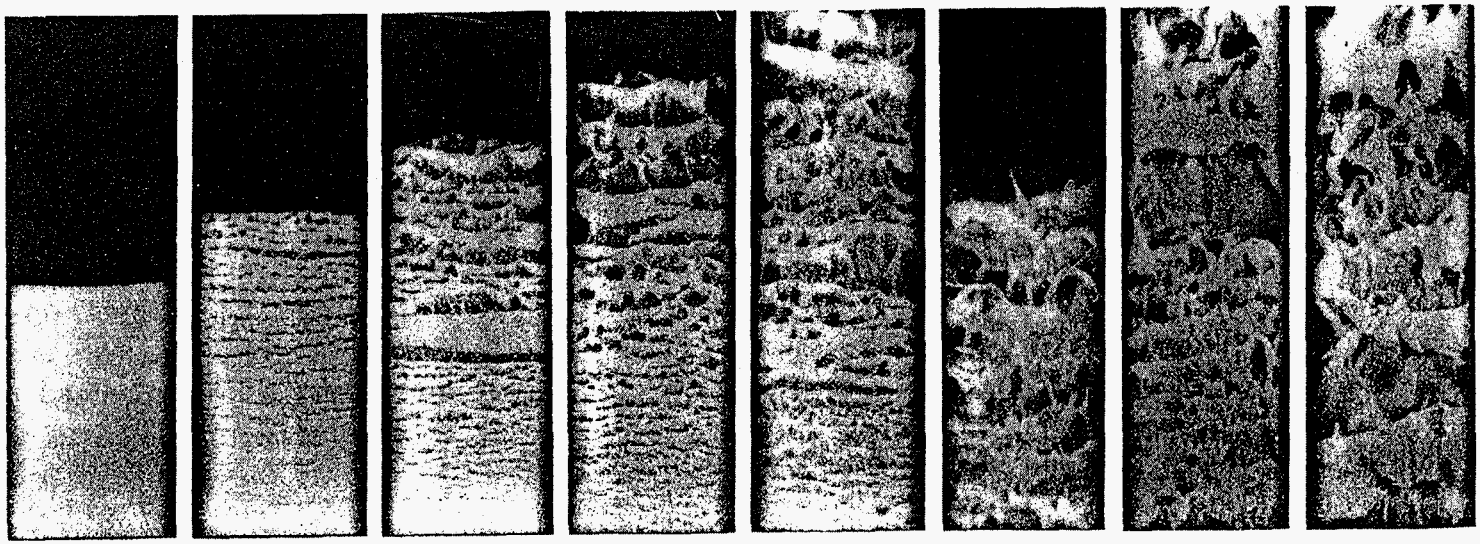

Fig. 31

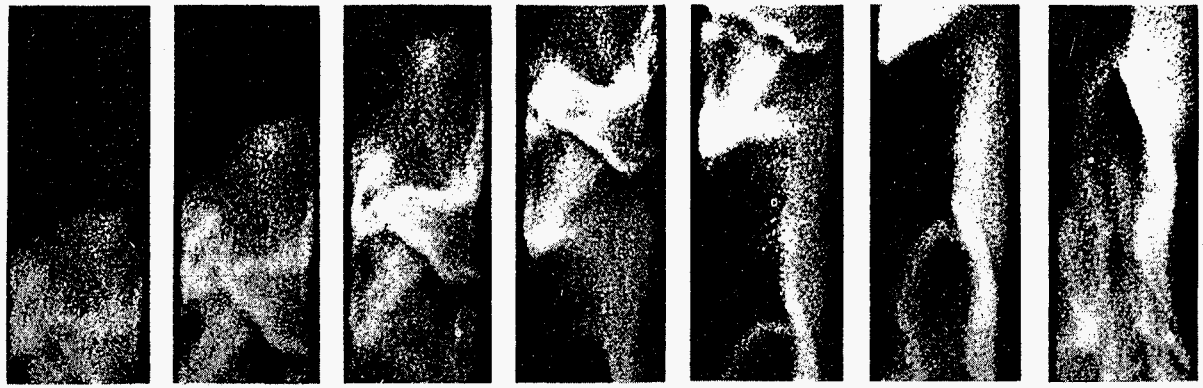

Fig. 32

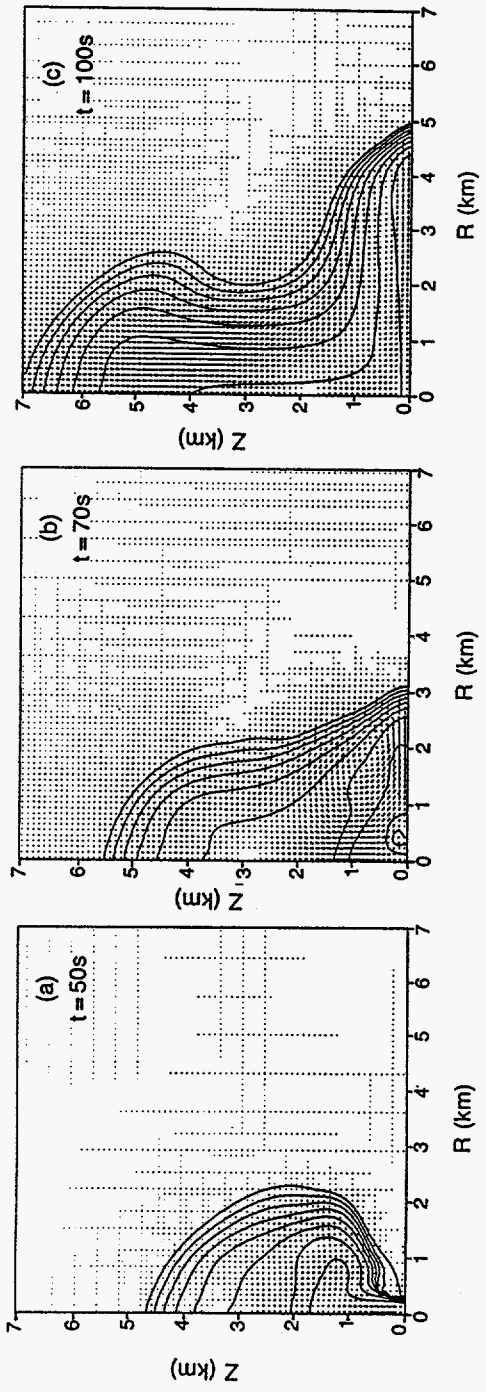

Fig. 33

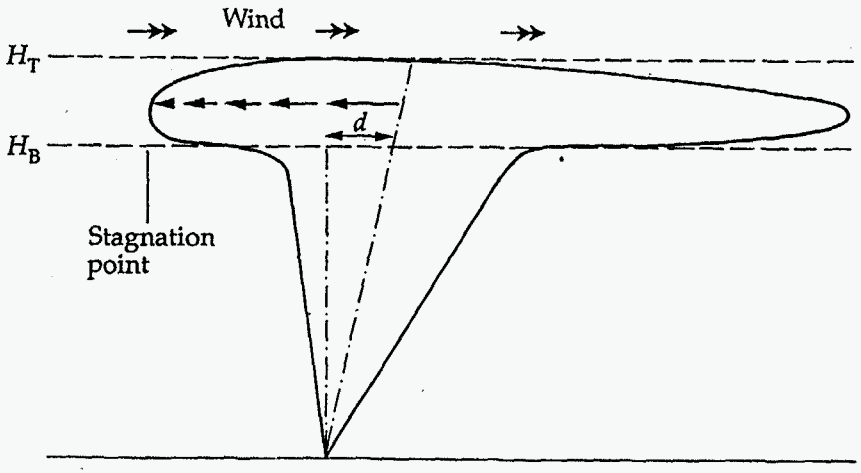

Upwind stagnation point and displacement of plume axis in an eruption column. Arrows within plume show velocity vectors in spreading region; where spreading velocity is balanced by equal and opposite wind velocity (double arrowed vectors) defines stagnation point. The d is displacement of column axis. In cases where the amount of upwind spreading is the same as column displacement, the upwind edge of the column is vertical.

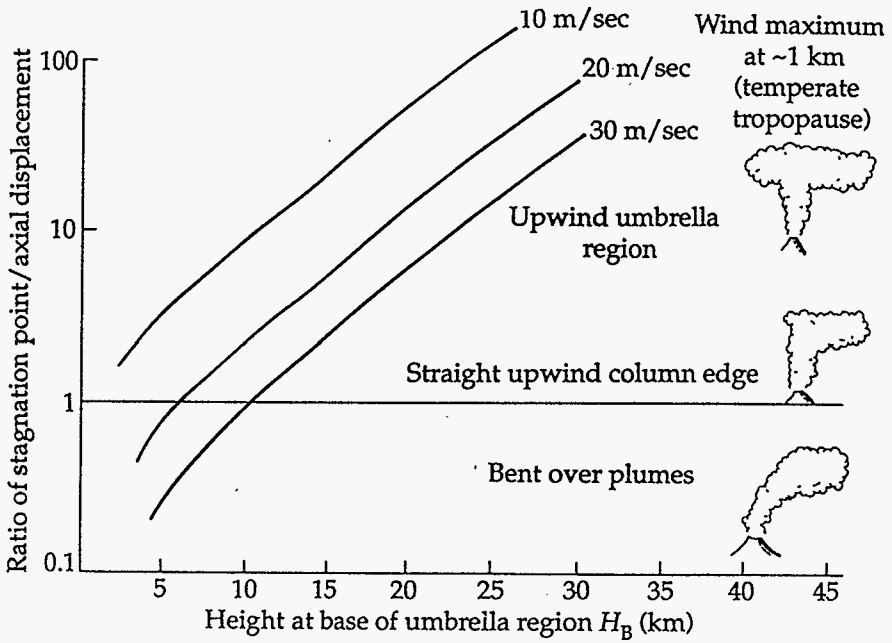

Ratio of distance to stagnation point to axial displacement plotted against column height H_B for wind speeds of 10, 20, and 30 metres per second, showing contrasted shapes of plumes. From Carey, S. and Sparks, R. S. J. (1986) Quantitative models for the fall-out and dispersal of tephra from volcanic eruption columns. *Bull. Volcanol.* **48**, 109–25.

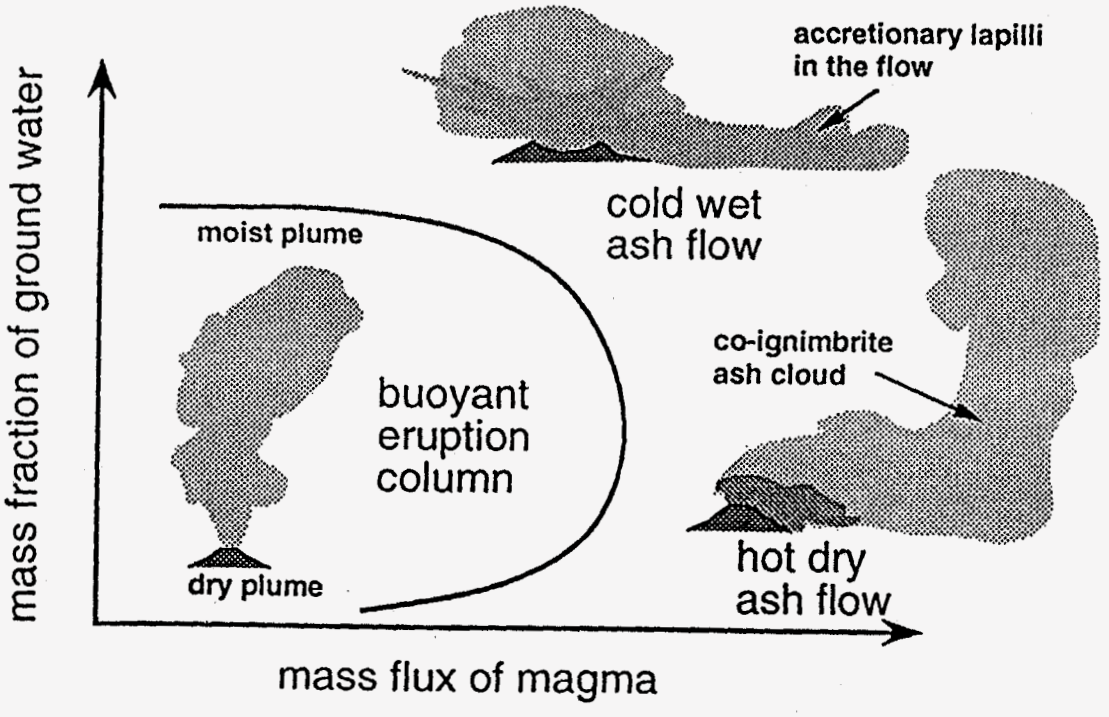
accretionary lapilli
in the flow
cold wet
ash flow
moist plume
buoyant
eruption
column
co-ignimbrite
ash cloud
dry plume
hot dry
ash flow
mass fraction of ground water
mass flux of magma

Fig. 36